PNNL-30041

Light Water Reactor Sustainability Program

Sequential versus Simultaneous Aging of XLPE and EPDM Nuclear Cable Insulation Subjected to Elevated Temperature and Gamma Radiation

June 2020

U.S. Department of Energy

Office of Nuclear Energy

PNNL-30041

Sequential Versus Simultaneous Aging of XLPE and EPDM Nuclear Cable Insulation Subjected to Elevated Temperature and Gamma Radiation

Leonard S. Fifield Mychal P. Spencer
Andy Zwoster Tucker T. Bisel Mark K. Murphy

June 2020

Prepared for the
U.S. Department of Energy
Office of Nuclear Energy

SUMMARY

This report addresses one of the knowledge gaps identified for the prediction of nuclear electrical cable aging, accelerated aging, performed during cable qualification. Synergistic effects are defined as polymer aging mechanisms specific to simultaneous or concurrent application of thermal and gamma radiation. If these effects differ from those experienced during sequentially applied thermal and gamma radiation stressors, then qualification that relies on sequential aging, as most historically did, may not well represent actual service aging when stressors exist simultaneously.

In this report, two of the most common cable insulation materials used in nuclear containment—cross-linked polyethylene (XLPE) and ethylene-propylene-diene elastomer (EPDM)—were selected to assess the relevancy of the findings. Accelerated aging experiments were conducted while holding both the dose rate and temperature constant to better understand cable degradation based upon the order of sequence of the stressor. The dose rate, total doses, and temperature used were selected based on input from multiple expert stakeholders and based on experimental constraints. Characterization methods that include mass change, elongation at break, carbonyl index, total color difference, and density were selected to quantify the severity of the selected aging scenarios: (1) simultaneous [*T/R*, thermal and irradiation], (2) sequential [*T+R*, thermal followed by irradiation], and (3) sequential [*R+T*, irradiation followed by thermal].

The characterization results yielded insights into lifetime prediction of low-voltage nuclear instrumentation cables. Most significantly, sequential aging was found to produce a significantly different operational lifetime (defined as time to 50% of the unaged specimen elongation at break) when compared to simultaneous aging depending on the insulating material type and aging scenario. For XLPE, lifetimes were found to be less than the simultaneous aging scenario for the sequential thermal followed by irradiation aging, but greater for the sequential irradiation followed by thermal aging. Conversely, for EPDM, lifetimes were found to be less than the simultaneous aging scenario for sequential irradiation followed by thermal aging, but greater for sequential thermal followed by irradiation aging. This report also demonstrates that mass change may be a useful technique for estimating the degradation of cables insulated with EPDM, particularly with the simultaneous and sequential irradiation followed by thermal aging scenarios, because a sharp decrease in mass was observed to correlate to a reduction in elongation at break. In addition, the carbonyl index for XLPE and the total color difference for EPDM were observed to be possibly advantageous non-destructive characterization methods to estimate cable insulation lifetimes.

Understanding material-specific aging mechanisms, differences between laboratory accelerated aging and in-plant service aging, and identifying the most effective methods for non-destructively tracking aging are important for long-term nuclear power plant operations. This knowledge can guide cable aging management programs and re-licensing activities by prioritizing cable replacement decisions for cost-effective, efficient, and safe operation.

ACKNOWLEDGEMENTS

This work was sponsored by the U.S. Department of Energy, Office of Nuclear Energy, for the Light Water Reactor Sustainability (LWRS) Program Materials Research Pathway. The authors extend their appreciation to Pathway Lead Dr. Thomas Rosseel for LWRS programmatic support. This work was performed at the Pacific Northwest National Laboratory (PNNL). PNNL is operated by Battelle for the U.S. Department of Energy under contract DE-AC05-76RL01830.

CONTENTS

FIGURES

TABLES

ACRONYMS

ASTM	American Society for Testing and Materials
ATR	attenuated total reflectance
CI	carbonyl index
CIE	Commission on Illumination
CSPE	chlorosulfonated polyethylene
DLO	diffusion limited oxidation
EAB	elongation at break
EPDM	ethylene-propylene-diene elastomer
EPR	ethylene-propylene rubber
ETFE	ethylene tetrafluroethylene
EMDA	Expanded Materials Degradation Assessment
FTIR	Fourier-transform infrared spectroscopy
HEF	High Exposure Facility
IEC	International Electrotechnical Commission
IEEE	Institute of Electrical and Electronics Engineers
ISO	International Standards Organization
LWRS	Light Water Reactor Sustainability
NPP	nuclear power plant
NIH	National Institute of Health
OIT	oxidation induction time
PE	polyethylene
PNNL	Pacific Northwest National Laboratory
PVC	polyvinyl chloride
R	radiation-only aging
R+T	sequential aging (irradiation followed by thermal)
ROI	region of interest
SR	silicone rubber
sRGB	standard red-green-blue
T	temperature-only aging
T+R	sequential aging (thermal followed by irradiation)
T/R	simultaneous aging (thermal and irradiation)
XLPE	cross-linked polyethylene

1. INTRODUCTION

Approximately 20% of the power produced in the United States comes from nuclear power plants (NPPs) [1]. Originally, NPPs were qualified for a minimum operational lifetime of 40 years [2,3]. As described in the foreword of the U.S. Nuclear Regulatory Commission's (NRC's) Expanded Materials Degradation Assessment (EMDA) Volume 5: Aging of Cables and Cable Systems [4], and according to Title 10 of the Code of Federal Regulations, Part 54 (10 CFR 54), Requirements for Renewal of Operating Licenses for Nuclear Power Plants," NPPs can apply for 20-year license extensions following the original 40-year operating period. While a number of NPPs have already entered their extended lifetimes of up to 60 years, consideration is now being given to extend licenses an additional 20 years for up to 80 years of operational lifetime [5]. The viability of a second license renewal is dependent upon the NPPs operating safely in accordance with the licensing basis established with the original 40-year license. Hence, the NRC has developed aging management program requirements to promote the safe function of NPPs over these license extensions. The EMDA report identified cable aging-related issues that may be important for the second license renewal of NPPs.

Based upon the issues raised in EMDA Volume 5, a U.S. Department of Energy-sponsored research and development roadmap workshop report [6], and additional emerging issues, Pacific Northwest National Laboratory (PNNL) prioritized a list of 11 cable-aging knowledge gaps [7]. From this list, four knowledge gaps were selected for investigation as described by Fifield et al. [7], including the following: (1) diffusion limited oxidation (DLO) effects due to oxygen permeability hindrance at the polymer surface [8,9], (2) dose-rate effects where polymer degradation is not only a function of total absorbed dose, but also of the dose rate [10], (3) inverse temperature effects in which degradation due to gamma irradiation is lower at lower temperatures [11], and (4) synergistic effects due to the combined interactions between temperature and radiation [12,13]. Of these four cable knowledge gaps, the focus of this report is on the "synergistic effects."

Arguably, synergistic effects are the least well understood cable knowledge gap [14] because the interaction between temperature and radiation are not additive, but coupled. To better understand synergistic effects, Ito modified the Arrhenius equation by correlating the first-order rate constant as the superposition of rate constants due to temperature, radiation, and a coupling between temperature and radiation [15]. More recent work by Gillen extended this approach to systems with non-first-order behavior, a set that includes most materials [12]. However, even using these approaches, estimation of the rate constant, which is necessary to predict cable insulation lifetimes in synergistic aging scenarios, is difficult because the stress order also influences the rate constant. Because initial qualification of NPP cable insulation was historically conducted using a sequential aging scenario (thermal aging followed by irradiation), instead of the more realistic simultaneous aging scenario (thermal aging combined with irradiation), there are uncertainties regarding how conservative these accelerated aging tests were [16].

In this report, two common nuclear cable insulation materials [2]—cross-linked polyethylene and ethylene-propylene-diene elastomer—were aged simultaneously and sequentially at a constant dose rate and temperature to evaluate potential synergistic effects [7]. A variety of characterization techniques were employed to assess the aging scenarios and supply more complete information to regulators, operators, and other decision-makers about the long-term operation of nuclear cables exposed to synergistic effects. First, in Section 2, the two cable insulation materials investigated are described. Then, in Section 3, accelerated aging involving elevated temperature and gamma radiation applied to the insulation samples is described. In Section 4, information is provided about the methods used to characterize changes in the insulation materials upon aging, including mass, tensile elongation at break, carbonyl index, total color difference, and density. Section 5 contains a discussion the theory of polymer degradation related to the conditions employed. Characterization results are provided in Section 6, followed by a discussion of results in Section 7. Finally, concluding remarks are made in Section 8.

2. MATERIALS

To assess the relevance of the findings of this report, the materials characterized were selected based upon those commonly found within nuclear containment [2]. Subsequently, both cross-linked polyethylene (XLPE) and ethylene-propylene-diene elastomer (EPDM)[1] were selected for analysis of the order of sequence and synergistic effects because insulation material types similar to these are present within at least 75% of nuclear containments in U.S. NPPs, as shown in Table 1. In addition to the selected material type, low-voltage nuclear grade instrumentation cables were selected because approximately 81% of electrical cables within U.S. NPPs are low-voltage instrument and control cables [17]. Manufacturer information for the selected cables is shown in Table 2.

Table 1. The most common nuclear cable insulation and jacket material types within containment [2]; values shown are approximations.

Material	Percent of Units (%)
XLPE	90
EPDM/EPR	75
SR	27
CSPE	24
ETFE	15
PVC	7
PE	3
Neoprene	3
Polyimide	3
Polyalkene	2

XLPE = cross-linked polyethylene; EPDM = ethylene-propylene-diene elastomer; EPR = ethylene-propylene rubber; SR = silicone rubber; CSPE = chlorosulfonated polyethylene; ETFE = ethylene tetrafluoroethylene; PVC = polyvinyl chloride; PE = polyethylene.

Table 2. The nuclear grade instrumentation cables used in this study.

Manufacturer	Product Identifier	Sourced From	Jacket Material	Insulation Material
RSCC Wire & Cable	I46-0021	Manufacturer	CSPE	XLPE
Samuel Moore Group	Dekoron® 2/C 16 AWG 600 V	Electric Power Research Institute (EPRI)	CSPE	EPDM

CSPE = chlorosulfonated polyethylene; XLPE = cross-linked polyethylene; AWG = American Wire Gauge; EPDM = ethylene-propylene-diene elastomer.

The white insulation was extracted from the electrical instrumentation cables of Table 2 by first carefully removing the chlorosulfonated polyethylene (CSPE) jackets. Next, a wire stripping tool was used to mark the insulation in 100 mm increments. Afterwards, the exposed conductors (see Figure 1 for an example) were fixed in place with a vice and the insulation was removed by gently pulling the

[1] In EPDM, E refers to ethylene, P to propylene, D to diene, and M to the material's classification as a rubber "having a saturated chain of the polymethylene type" in ASTM International (ASTM) D1418 [18]. (The Vanderbilt Rubber Handbook, 14th Edition. Edited by Martin F. Sheridan. 2010 [19]).

insulation over the conductors. The extracted insulation was 100 mm in length. The tubular cross-sections were measured as 4.74 mm^2 (1.28 ± 0.04 mm inner diameter and 2.79 ± 0.08 mm outer diameter) and 4.64 mm^2 (1.35 ± 0.07 mm inner diameter and 2.78 ± 0.04 mm outer diameter) for the XLPE and EPDM insulations, respectively.

The material types of the extracted insulation were confirmed by comparing their absorbance spectra to literature data using Fourier-transform infrared spectroscopy (FTIR). The spectra of the as received, or unaged, insulation specimens are shown in Figure 2. Due to their chemical structure, methylene absorption (-CH_2-) is useful for identification of both XLPE and EPDM. For both material types, strong characteristic methylene asymmetric and symmetric stretching absorbance peaks were measured at 2916 cm^{-1} and 2848 cm^{-1}, respectively [20,21]. In addition, both material types demonstrate characteristic methylene bending modes at 1462 cm^{-1} (scissoring), 1349 cm^{-1} (wagging), and 729 cm^{-1} (rocking), similar to those observed in the literature [22–24]. Absorption was observed for the unaged EPDM specimen at 1050 cm^{-1}, likely due to trans hydrogen atoms on a double bond—an artifact of the vulcanization process [25]. Furthermore, absorption of trans-substituted [26] and tri-substituted [27] alkenes were found at 866 cm^{-1} and 808 cm^{-1} for the unaged EPDM specimen, respectively. Both material types produced weak carbonyl bonds in the range of 1600 to 1720 cm^{-1}, likely due to oxidation.

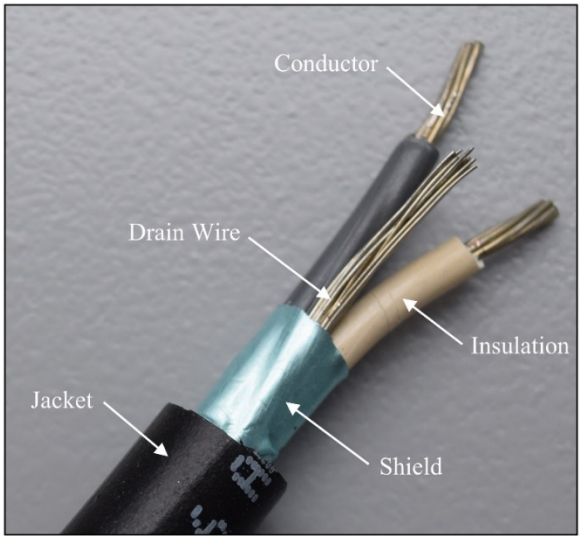

Figure 1. Exposed conductors within an exemplary low-voltage nuclear grade instrumentation cable.

Location	K (cm^{-1})	Functional Groups
(1)	2916	CH_2 asymmetric stretch
(2)	2848	CH_2 symmetric stretch
(3)	1720	C=O stretch
(4)	1462	CH_2 scissoring
(5)	1349	CH_2 wagging
(6)	1050	Trans hydrogen
(7)	866	Trans-substituted alkene
(8)	808	Tri-substituted alkene
(9)	729	CH_2 rocking

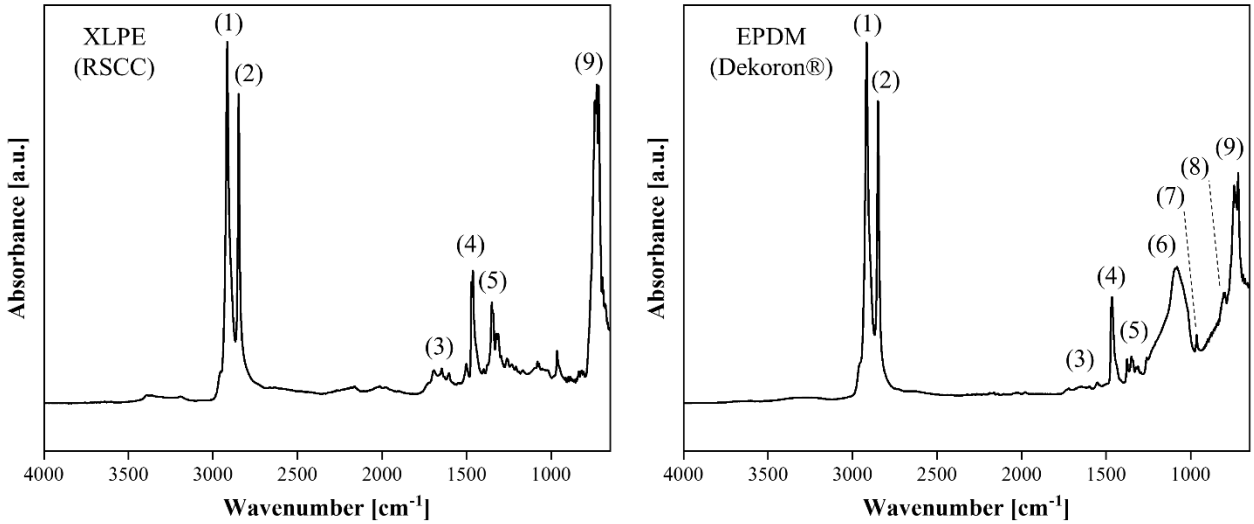

Figure 2. FTIR absorbance spectrum of the white as-received (left) XLPE and (right) EPDM low-voltage nuclear grade cable insulation.

3. SIMULTANEOUS AND SEQUENTIAL THERMAL/GAMMA AGING

Prior to aging, the mass of each insulation specimen was measured. Each specimen was then attached to a clip labeled with a unique specimen identifier, as shown in Figure 3. Afterwards, the specimens were hung from a rack and exposed to one of three aging scenarios:

1. *T/R*: simultaneous heating at 150°C and gamma irradiation at 300 Gy/hr
2. *T+R*: heating at 150°C for a designated duration followed by gamma irradiation at 300 Gy/hr for the same duration
3. *R+T*: irradiation at 300 Gy/hr without heating for a designated duration followed by heating at 150°C for the same duration.

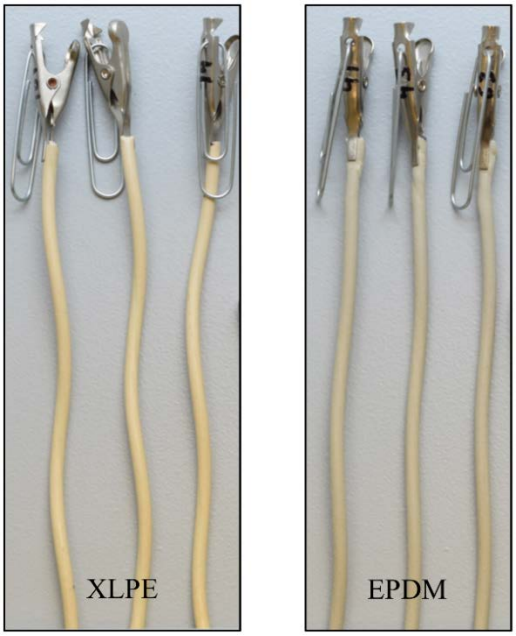

Figure 3. Extracted, labeled, and clipped insulation specimens prior to aging.

To evaluate the effects of the order of sequence on insulation degradation, the dose rate, total dose, and the temperature were held constant for each aging scenario and test condition. Using an approximately 11000 Ci Cobalt-60 (Co-60) source, gamma irradiation was conducted at the High Exposure Facility (HEF) at PNNL. The dose rate was held constant by positioning the specimens at 56 cm from the Co-60 source. The temperature was controlled through integrated thermocouple feedback and provided by a mechanical convection oven, as shown in Figure 4; the oven was modified to enable the heating elements to be independent of the oven fans to maintain air circulation in the absence of heating. With no heating, the ovens were at an ambient temperature of 26°C. The test conditions for each aging scenario described above are shown in Table 3. The 150°C temperature and 300 Gy/hr dose rate were selected based on time constraints for the exposure experiment, to achieve the radiation exposure of all three scenarios (T/R, T+R and R+T) within the approximately 120 days of irradiation time available for the particular campaign at the HEF. It is acknowledged that DLO is likely to occur to some extent at temperatures above 130°C and at dose rates above 100 Gy/hr, but the complicating effects of DLO are not considered here. Unaged specimens were evaluated for benchmark reference.

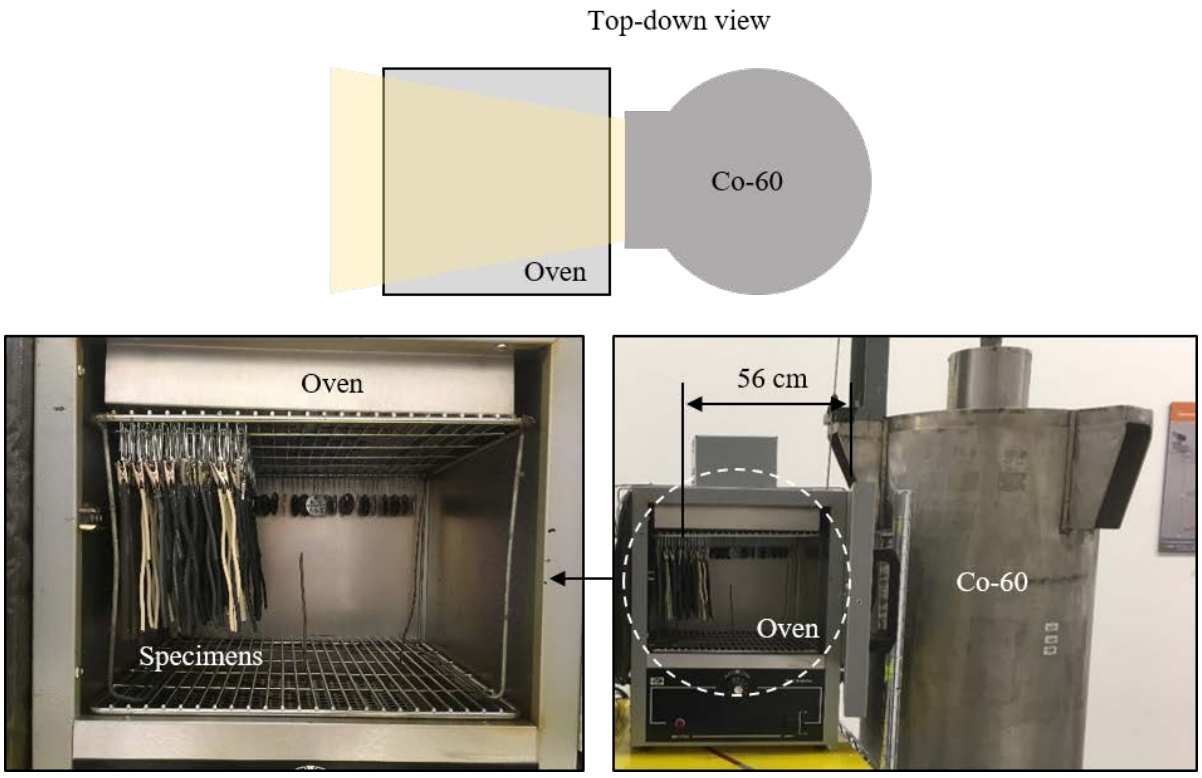

Figure 4. Clipped insulation specimens hung in the oven located at the HEF facility.

Table 3. Evaluated test conditions for sequential versus simultaneous exposure of nuclear grade XLPE and EPDM insulation cable.

Test Condition	Dose (kGy)	Exposure (Days)
1	Unaged	
2	20	3
3	40	5
4	60	9
5	150	21
6	170	23
7	260	36
8	280	39
9	300	41
10	320	44

4. EXPERIMENTAL METHODS

To investigate the effects of simultaneous (*T*/*R*) aging, in comparison to sequential aging (*T*+*R*, *R*+*T*), on the degradation behavior of the insulation specimens, five different characterization methods were employed as discussed below.

4.1 Mass Measurement Using an Analytical Balance

An analytical balance (Fisher Scientific ALF104, ± 0.001 g resolution, see Figure 5) was used to measure the mass of the insulation specimens before and after aging. In addition, the mass was measured after the first aging cycle for the sequential aging scenarios (after thermal for *T*+*R* and after radiation for *R*+*T*). The masses of three insulation specimens were measured for each aging condition.

Figure 5. Fisher Scientific ALF104 analytical balance used to measure insulation mass.

4.2 Elongation at Break Measurement Using Video Extensometry

Following IEC/IEEE 62582-3, the tensile elongation at break (EAB) was measured for the aged insulation specimens. Table 4 lists the test parameters for both material types. For each aging condition, the insulation specimens were cut to a length of 45 mm and the inner and outer diameters were measured using a digital caliper. A black permanent marker with a fine tip size was used to draw two gauge marks centered and at 20 mm separation on the insulation specimens. Afterwards, the insulation specimens were conditioned following ASTM D618 Procedure A: at least 40 hours at 23°C ± 2°C and 50% ± 10% relative humidity. The humidity was controlled by placing the specimens in a covered desiccator subjected to a saturated solution of potassium carbonate and deionized water (fixed humidity point of 43% [28]). A data logger (Omega OM-EL-USB-2-LCD-PLUS) was placed in the desiccator to monitor both the temperature and humidity. After conditioning, end tabs of 5 mm length were gently slipped over the ends of the specimens with an approximate gap of 2 mm between the ends of the specimens and the end tabs (see Figure 6A). The method of attachment of the end tabs to the specimen depended upon the material type: the end tabs were gently compressed prior to placement on the XLPE specimens and two layers of tissue (Kimtech Science Kimwipes) were placed between the specimen and end tabs to avoid slippage of the end tabs on the EPDM specimens. After attachment of the end tabs, the specimens were placed centered and along the axis of a pair of pneumatic grips at a separation of 30 mm. A testing rate lower than that specified in IEC/IEEE 62582-3 was incorporated to avoid early failure of the specimens. As shown in Figure 6B, a tensile testing machine (Instron® 3360 Universal Testing System, Norwood, MA) was used to apply tension to the specimens.

Table 4. Test parameters for EAB measurement.

Material Type	Test Rate (mm/min)	End Tab Material	Grip Pressure (psi)
XLPE (RSCC)	10	XLPE (Grainger, 10A671)	60
EPDM (Dekoron®)	20	CSPE (RSCC, I46-0021 Jacket)	40

CSPE = chlorosulfonated polyethylene; EPDM = ethylene-propylene-diene elastomer; XLPE = cross-linked polyethylene.

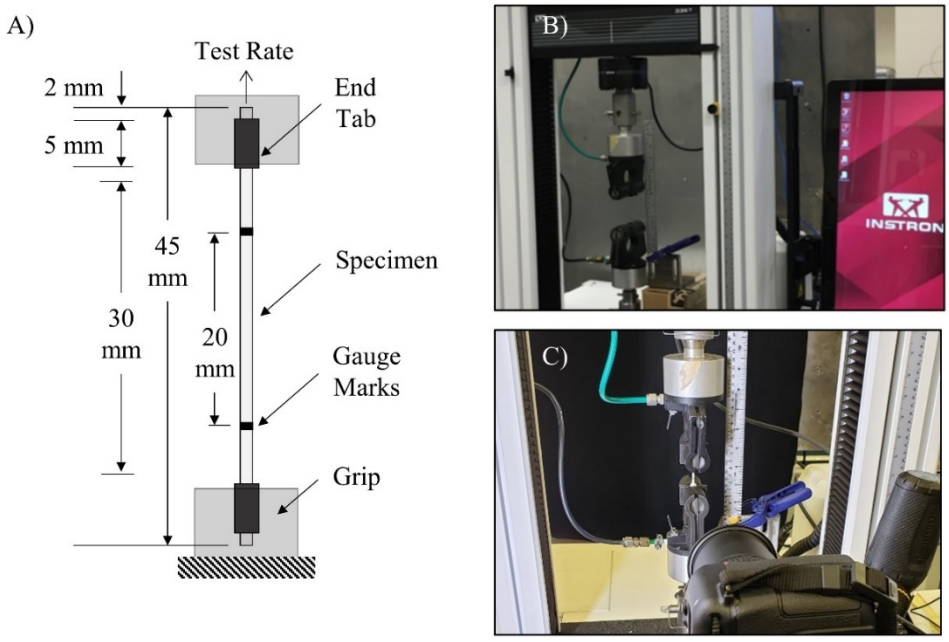

Figure 6. A) Testing schematic for video extensometry of the insulation specimens and digital images of the B) test frame and C) digital camera positioning.

For each aging condition, the EAB was video recorded. As shown in Figure 6C, a tripod was used to mount and orient a digital camera (Nikon D7500) such that the entire extension of the specimens could be captured. The settings of the digital camera were optimized to enhance video extensometry processing: 1080p resolution to reduce file size, 1/250 s exposure time to ensure clean break frame detection, an aperture of f10 to enhance the depth of field, and an ISO setting of 1000 to balance specimen illumination and background noise. Specimen lighting was controlled by placing two light sources (Genaray SP-S-1000D, 100% illumination) behind and to either side of the camera and directing the light towards the specimens. In addition, edge detection during video processing was enhanced by the placement of a diffuse black background behind the specimens. Video recording was started prior to elongation of the specimen and stopped immediately upon failure of the specimen.

After video recording, each video was processed using an in-house-developed video extensometry code written in MATLAB (MathWorks®, Natick, MA) and R (The R Foundation, r-project.org). The videos were analyzed following the process shown in Figure 7. The elongation (%) [29] was calculated as shown in Equation (1), where E_0 and E_c are the starting and current gauge length (based on pixel location), respectively. The final elongation measured was recorded as the EAB.

$$e = 100\frac{E_c - E_0}{E_0} \quad (1)$$

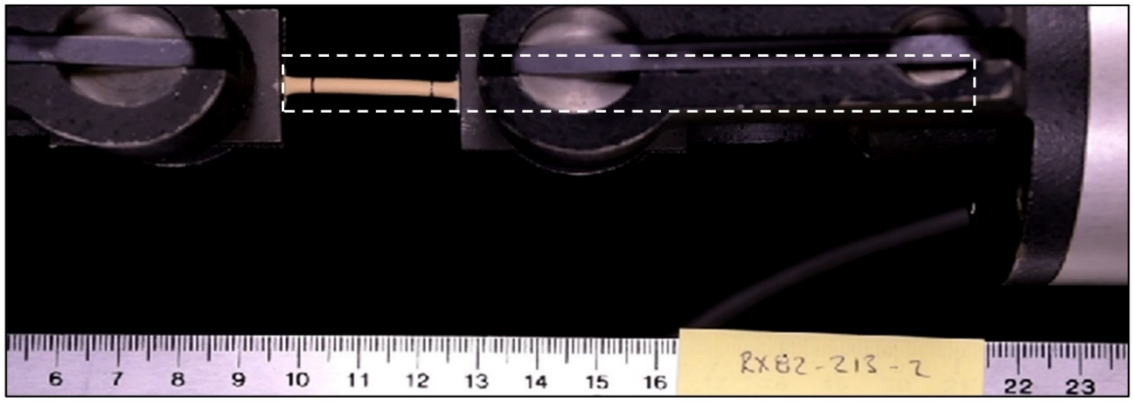

A) Example output frame from the digital camera during specimen elongation.

B) Frames were cropped (--- line shown above), converted to greyscale, thresholding was applied (pixels < 25 set to 25), and a 3x3 median filter applied to reduce noise.

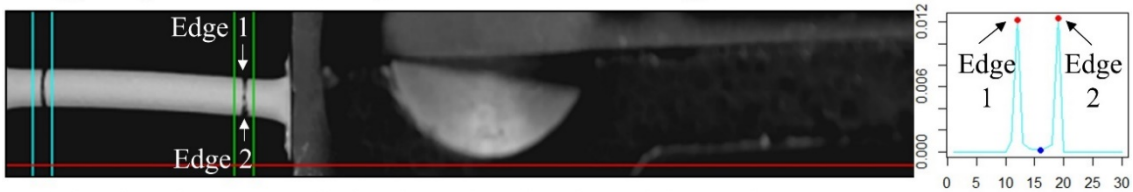

C) Edge detection was applied to determine the edges of the specimens.

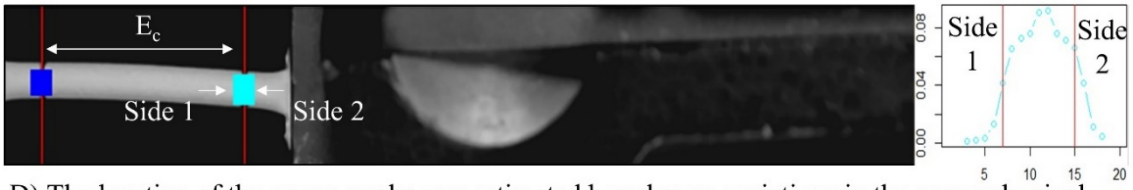

D) The location of the gauge marks was estimated based upon variations in the greyscale pixel intensity. The distance between gauge marks (in pixels) was stored for each frame.

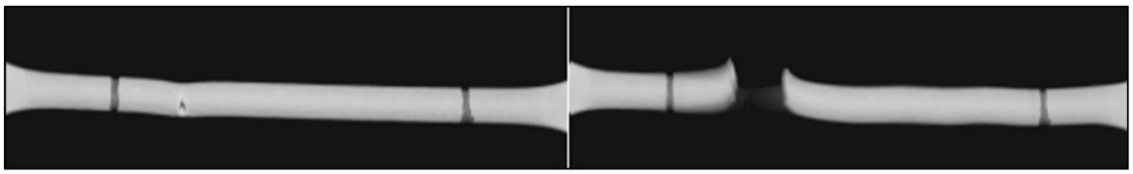

E) A frame-to-frame increase in the gauge length by more than 15 pixels was specified as the break frame.

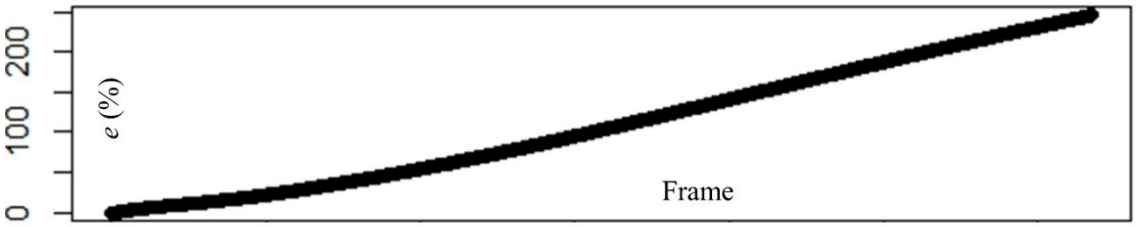

F) For each frame the elongation was measured. After specimen failure, the elongation curve was smoothed using locally weighted scatterplot smoothing.

Figure 7. Process for analyzing insulation specimens using video extensometry.

4.3 Carbonyl Index Measurement Using FTIR

FTIR attenuated total reflectance (ATR) (Thermo Scientific Nicolet iS10) was used to measure the carbonyl index of the aged insulation specimen external surfaces. Approximately 5 mm was extracted from the end of each insulation specimen for FTIR analysis. Specimen surfaces were gently cleaned with deionized water after aging to minimize surface contamination because FTIR ATR is a surface sensitive technique (for example, penetration depths are typically on the order of 4 µm at 500 cm^{-1} and 0.5 µm at 4000 cm^{-1} for XLPE and a diamond ATR crystal [30]). After cleaning, the specimens were conditioned following the same procedure as described in Section 4.2 (at least 40 hours at 23°C ± 2°C and 50% ± 10% relative humidity). A background spectrum was collected prior to measurement for spectra subtraction. To enhance the measured absorbance values, an anvil tool was used to compress the specimens against the diamond ATR crystal to ensure complete contact, see Figure 8. A total of 64 scans were collected for each measurement to reduce background noise. In addition, to account for variation based upon measurement location, a spectrum was collected at two locations on each specimen surface.

Analysis of the spectra peaks was conducted using OriginPro software (OriginLab®, Northampton, MA). Peak absorbance intensities corresponding to the methylene group (2848 cm^{-1}, CH_2 symmetric stretching [31]) and carbonyl group (1715 cm^{-1}, C=O stretch [32]) were recorded from a baseline as shown in Figure 9. The carbonyl index is given in Equation (2), where H_{2848} and H_{1715} are the peak absorbance intensities for the methylene and carbonyl groups, respectively.

$$CI = \frac{H_{1715}}{H_{2848}} \tag{2}$$

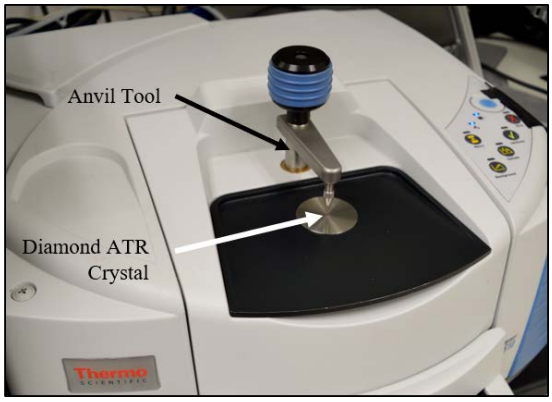

Figure 8. Thermo Scientific Nicolet iS10 FTIR with ATR adapter used to measure carbonyl index.

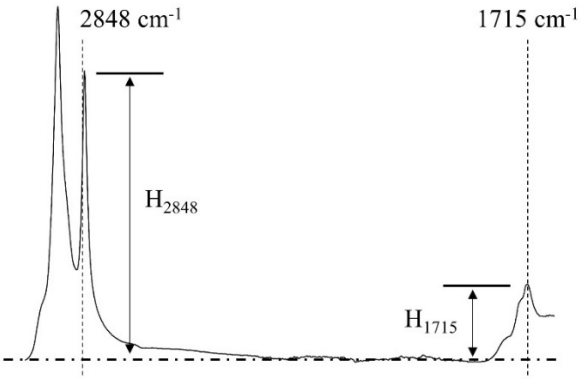

Figure 9. Example FTIR spectrum for EPDM insulation demonstrating the measurement methodology.

4.4 Total Color Difference Measurement Using a Digital Camera

Polymeric specimens darken upon aging when exposed to thermal and radiation stressors. Following ASTM D1729 and ASTM D2244, the total color difference (ΔE^*_{ab}) of the aged insulation specimens was measured using a light booth (GTI MiniMatcher MM 2e) and digital camera (Nikon D5300). A clamp was used to fix the digital camera in place and orient the camera lens perpendicular to the display plane of the light booth (see Figure 10). To optimize collected image quality, the digital camera settings were as follows: an exposure time of 1/3 s to enhance color saturation, an aperture of f14 to enhance depth of field, and an ISO setting of 100 to reduce background noise. A wireless remote control (Nikon ML-L3) was used to ensure the camera did not move during image collection and to facilitate batch processing. In the light booth, a standard International Commission on Illumination (CIE) D65 light was used; background lighting in the room was extinguished during image collection. To facilitate image calibration and conversion to the CIE XYZ color space (and subsequently the L*a*b* color space [defined below]), a color reference target was placed on the light booth display plane. The aged insulation specimens were placed next to the color reference target as shown in Figure 11A. Because of the issues with surface reflections on tubular specimens and variations in color along the specimen lengths, each insulation specimen was removed after image collection, rotated slightly, and then returned next to the color reference target before another image was captured. This process was repeated twice for a total of three images per insulation specimen.

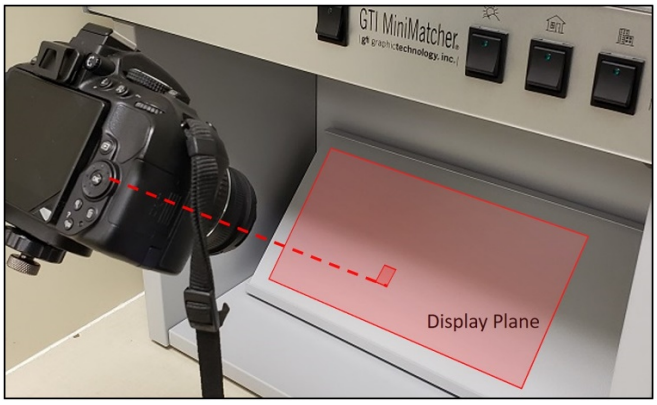

Figure 10. Digital camera and light booth orientation for total color difference image collection.

Due to their inherent components and internal processing, a digital camera and lens will modify the color in digital images; therefore, it is necessary to map these modified colors into a system with an absolute measure of color prior to quantifying color changes. ImageJ (NIH) was used in conjunction with the micaToolbox [33,34] to convert the collected images to the CIE XYZ color space. First, the six grey standards located on the bottom row of the color reference target (see Figure 11A) were converted to reflectance values using manufacturer-supplied standard Red Green Blue (sRGB) triplets for each grey standard and then using an iterative least log slope approach [35] to convert the triplets to reflectance values. Second, the grey reflectance values were used to create a linear normalized reflectance stack, or calibrated multispectral image, for each collected image. Third, regions of interest (ROIs) were manually specified for each calibrated image, as shown in Figure 11B. Care was taken to select regions with no reflections or shadows and a total of three ROIs were selected for each image for a total of nine data points for each aging condition. Fourth, a cone-catch model [34] was generated based upon the charted reflectance spectra of the color reference target. Fifth, the cone-catch model was used to map the linear normalized reflectance stack to the CIE XYZ color space and the XYZ color space values of the ROIs were measured. Lastly, the measured XYZ color space values were mapped to D65 reference white point CIE L*a*b* color space through the built-in MATLAB function *xyz2lab*. The total color difference is

shown in Equation (3), where L^*_S, a^*_S, and b^*_S are the reference L*a*b* values and L^*_B, a^*_B, and b^*_B are the specimen L*a*b* values. The mean L*a*b values of the unaged specimens were selected as the reference values.

$$\Delta E^*_{ab} = \sqrt{(\Delta L^*)^2 + (\Delta a^*)^2 + (\Delta b^*)^2} \tag{3}$$

$$\Delta L^* = L^*_B - L^*_S$$

$$\Delta a^* = a^*_B - a^*_S$$

$$\Delta b^* = b^*_B - b^*_S$$

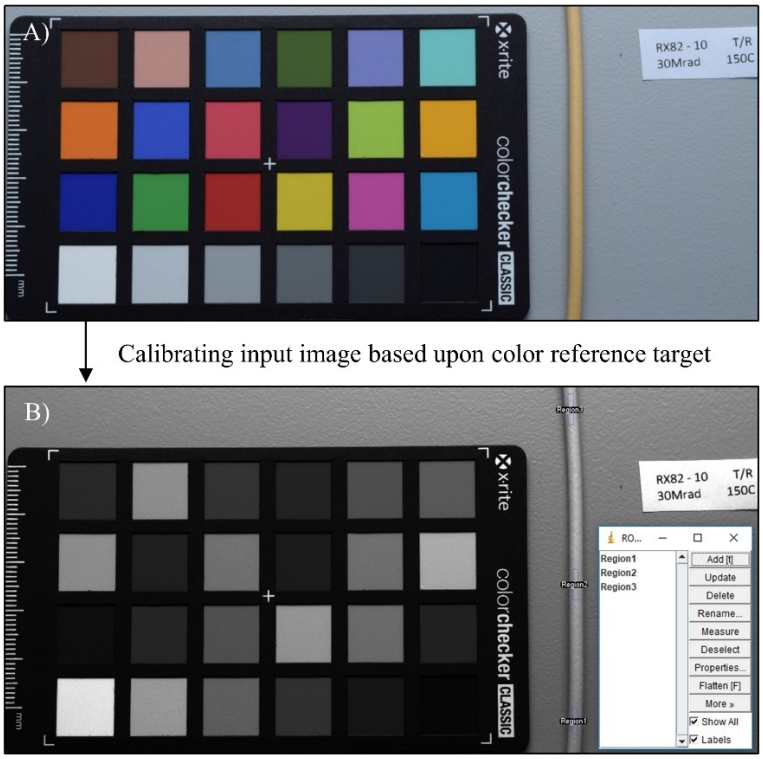

Figure 11. Conversion of the (A) input color image to a (B) multispectral calibrated image.

4.5 Density Measurement Using Archimedes' Principle

Following ASTM D792, the density of selected insulation specimens was measured. An approximate length of 5 mm was extracted from the end of the insulation specimens for density measurement. The specimens were conditioned following the same procedure described in Section 4.2 (at least 40 hours at 23°C ± 2°C and 50% ± 10% relative humidity). A high-resolution analytical balance (Sartorius CPA225D, ±0.0001 g) was used in conjunction with a density measurement kit (Sartorius YDK01) to measure the specimen mass in air and in water (see Figure 12). Prior to immersing the specimens, the mass of the specimens in air was measured. Afterwards, the specimens were wetted with isopropanol alcohol to limit the formation of air bubbles on the specimen surfaces. The specimens were then immediately placed in a convex sample holder immersed in deionized water (24.6°C ± 0.9°C); the sample holder was located at a depth of approximately 2.54 cm below the surface. The specimen apparent mass was then recorded, and the specimens were removed, again wetted with isopropanol, and set aside to dry. The above process was repeated two times for a total of three sets of measurements per insulation

specimen. The Archimedes' principle (water displacement) was used to determine the density, as shown in Equation (4) [36], where m is the average mass in air (g), m_l is the average mass immersed in water (g), and ρ_l is the density of the liquid (g/cm^3) at the measurement temperature.

$$\rho = \frac{m\rho_l}{m - m_l} \tag{4}$$

Figure 12. Sartorius CPA225D analytical balance used to measure insulation density.

5. POLYMER DEGRADATION THEORY

Oxidation is one of the primary degradation mechanisms for polymeric specimens undergoing combined thermal and radiation stress. Hardening at the specimen surface due to oxidation may lead to the initiation of cracks and their propagation through the material cross-section [12]. The generation of free radicals, and their consumption by any antioxidants that may be present within the polymer, affects the rate of oxidation which is also influenced by the aging scenario. For example, previous work has shown that the generation of free radicals may be the dominant mechanism for the simultaneous aging scenario, whereas free radicals may be predominantly consumed by antioxidants (until depleted) in the sequential aging scenario [37]. The use of first-order reaction kinetics has been routinely used to model the degradation of polymers [38]. As shown in Equation (5), the first-order system is composed of a rate term (k) dependent upon both temperature (T) and radiation dose (D), and a term correlating the fraction transformed or characteristic value (P) which is dependent on time (t).

$$-\frac{dP}{dt} = k(T,D)P(t) \tag{5}$$

Because the first-order differential equation shown in Equation (5) is separable and easily solvable, the solution is given by Equation (6), where P_0 is the initial characteristic value.

$$P(t) = P_0 e^{-k(T,D)t} \tag{6}$$

Here, instead of the first-order reaction model of Equation (5), a methodology based upon work in oxidation kinetics is suggested for modeling polymer degradation, specifically in correlation to polymer EAB. A sigmoidal trend has been previously observed in work investigating the thermal oxidation of polymers based upon chemiluminescence [39]: an initial induction period, followed by linear oxygen uptake, and finally depletion of oxidation reaction sites (free radicals). Work conducted by Celina and George [40] proposed that oxidation infected local zones within a polymer and then spread similar to the spread of infections during epidemics. The "infection" rate is shown in Equation (7), where P and (1-P) represent the "infected" and "uninfected" zones, respectively. While similar to the rate equation presented in Equation (5), the rate equation of Equation (7) is referred to as "mixed order" wherein the reaction is effectively first-order at low characteristic values and transitions to second-order at higher characteristic values.

$$-\frac{dP}{dt} = k(T,D)P(t)[P(t) - 1] \tag{7}$$

As the loss of elongation, or more specifically a reduction in the EAB (e_{EAB}), of a polymer specimen is correlated to its degree of oxidation [41], the above approach is incorporated as shown in Equation (8), where $e_{EAB,0}$ is the initial elongation at break prior to degradation and $e_{EAB}(t_c) = e_{EAB,0}/2$ is the time (t_c) at which EAB is half of its original value (the critical time). Equation (8) can be solved using separation of variables and its solution, given in Equation (9), is a sigmoidal decay starting at the initial EAB value and decreasing at a critical time with a slope dependent upon the rate term.

$$-\frac{de_{EAB}}{dt} = k(T,D)e_{EAB}(t)\left[e_{EAB}(t)/e_{EAB,0} - 1\right] \tag{8}$$

$$e_{EAB}(t) = \frac{e_{EAB,0}}{1+exp^{-k(T,D)\cdot(t-t_C)}} \tag{9}$$

Oxidation is commonly quantified using the carbonyl index for polyolefins because typical oxidation byproducts include the hydroxyl and carbonyl groups [42]. Previous work by Emanuel [43] demonstrated a power law correlation between the concentration of the carbonyl groups and aging time as shown in

Equation (10), where a is a constant related to the concentration of hydrocarbons and reaction probabilities and b is an exponential characteristic to the specimen and aging process. Recent work has shown variations in b between two and six, or even higher [42]. Furthermore, work in the literature has shown an initial nonlinear transient state, followed by a linear trend for the carbonyl index at total absorbed doses higher than 300 kGy [44].

$$CI = at^b \tag{10}$$

Another effect of aging on polymers is that their physical color can darken (white-to-yellow-to-dark yellow) due to chemical composition changes, such as the formation of carbonyl groups (oxidation), density variations of carbon clusters, or chain scission [45–47]. Due to the complexity of spectral variations with increasing degradation, quantification of color changes is difficult. Here, a simplified model based upon Equation (6) is incorporated as shown in Equation (11), where τ represents the rate, and c indicates the magnitude of the color change. An additional term, $\Delta E^*_{ab,\infty}$, representing the equilibrium color difference was added to Equation (6) to account for saturation of the degradation pathways (as $t \to \infty$, $\Delta E^*_{ab} \to \Delta E^*_{ab,\infty}$). Interestingly, this equation matches well with experimentally observed color intensity variations in polyethylene blends [48].

$$\Delta E^*_{ab} = \Delta E^*_{ab,\infty} + ce^{-\tau \cdot t} \tag{11}$$

6. RESULTS OF SIMULTANEOUS VERSUS SEQUENTIAL AGING CHARACTERIZATION

The characterization results for the simultaneous (*T/R*) and sequentially (*T+R*, *R+T*) aged insulation specimens are discussed below. For all figures, the error ranges were calculated as the standard deviation of the specimen measurements. In addition, for Figures 16, 19, and 21, curve fitting to the respective equations in Section 5 were conducted using OriginPro® software and the Chi-squared values were minimized.

6.1 Mass Change

The measured mass change of the insulation specimens after aging is compared to that of the unaged insulation specimens as shown in Figure 13; details regarding the mass change trends are summarized in Table 5. At 3 days of exposure (20 kGy), the *T+R*, *R+T*, and *T* (temperature only) aging scenarios produced an increase in specimen mass of approximately 2.5% for XLPE and 1.5% for EPDM. For both material types, the *T/R* and *R* (radiation only at 26°C) aging scenarios produced minor variations in mass at exposures less than 25 days (< 250 kGy); a small positive linear slope (between 1.1×10^{-2} to 4.0×10^{-3} percent per day of exposure) was measured for the *T/R* and *R* aging scenarios after the initial exposure (3 days, 20 kGy). However, at a higher exposure (36 days, 260 kGy) the *T/R* aging scenario produced a rapid, linear decrease in the measured mass for the EPDM specimens (an approximate drop of 3% from a dose of 260 kGy to 320 kGy), which correlates to a decrease in EAB measurements to be discussed next and in Section 7. A negative linear trend (between -1.6×10^{-2} to -5.3×10^{-2} percent per day of exposure) was observed for mass change in the *T+R*, *R+T*, and *T* aging scenarios after initial exposure (3 days, 20 kGy) for both material types, opposite to that found for the *T/R* and *R* aging scenarios. Similar to the *T/R* aging scenario, the *R+T* aging scenario for EPDM produced a rapid linear decrease (an approximate decrease of 9% from 170 kGy to 320 kGy) in the measured mass after 23 days of exposure (170 kGy).

Table 5. The linear slope in mass change after initial exposure (3 days); a second linear slope was observed for EPDM with the *T/R* and *R+T* aging scenarios after 23 days and 36 days of exposure, respectively.

Type	Aging Scenario	Initial (%)	Slope 1 (%/day)	Slope 2 (%/day)
XLPE (RSCC)	*T/R*	0.10	3.86×10^{-3}	--
	T+R	2.74	-1.57×10^{-2}	--
	R+T	2.41	-2.84×10^{-2}	--
	T	2.72	-3.44×10^{-2}	--
	R	0.08	1.08×10^{-2}	--
EPDM (Dekoron®)	*T/R*	-0.56	8.27×10^{-3}	-3.48×10^{-1}
	T+R	1.68	-1.88×10^{-2}	--
	R+T	1.06	-5.26×10^{-2}	-4.17×10^{-1}
	T	1.68	-4.89×10^{-2}	--
	R	-0.35	7.14×10^{-3}	--

EPDM = ethylene-propylene-diene elastomer; XLPE = cross-linked polyethylene.

The mass changes for each exposure step in the sequential aging scenarios are shown in Figure 14 for the effect of a radiation stressor after thermal aging and in Figure 15 for the effect of a thermal stressor

after irradiation. For both material types, a similar effect was observed with the application of radiation after thermal aging: the measured insulation mass increased by approximately 0.024% per day of exposure (or approximately $3.4x10^{-3}$ percent per absorbed kGy). Interestingly, this increase in mass is greater than that observed for irradiation alone (for example, a mass change of 0.011% and 0.0071% per day of exposure was measured for the *R* only aging scenario for XLPE and EPDM, respectively). On the other hand, differences were observed between the material types for thermal aging applied after irradiation, as illustrated by the sharp decrease in mass change for the EPDM specimens. For XLPE, with the application of thermal aging after irradiation, an initial increase in mass at low exposure (3 days, 20 kGy) was followed by a linear decrease in mass (-0.04% per day exposure). A similar linear decrease in mass was measured for EPDM up to 23 days exposure (-0.06% per day exposure), but a sharp linear decrease was measured after this exposure (-0.43% per day exposure after 23 days), which correlates to a sharp decrease in EAB.

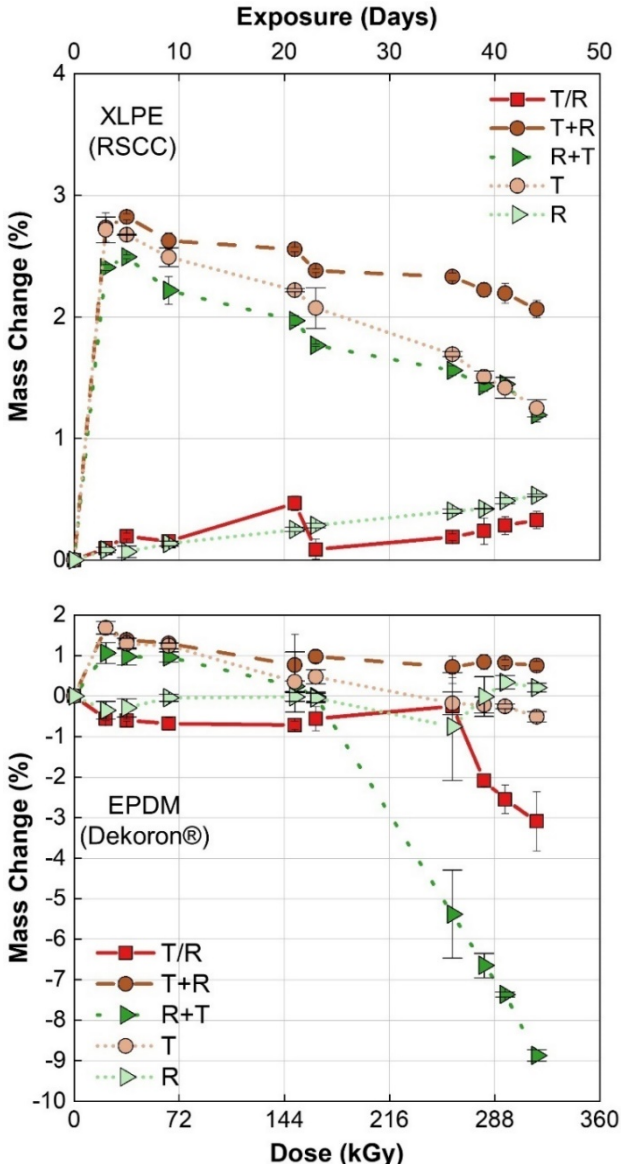

Figure 13. The average mass change of the (top) XLPE and (bottom) EPDM insulation specimens after aging. *T* represents thermal aging only (150°C) and *R* represents radiation aging at room temperature (26°C, 300 Gy/hr).

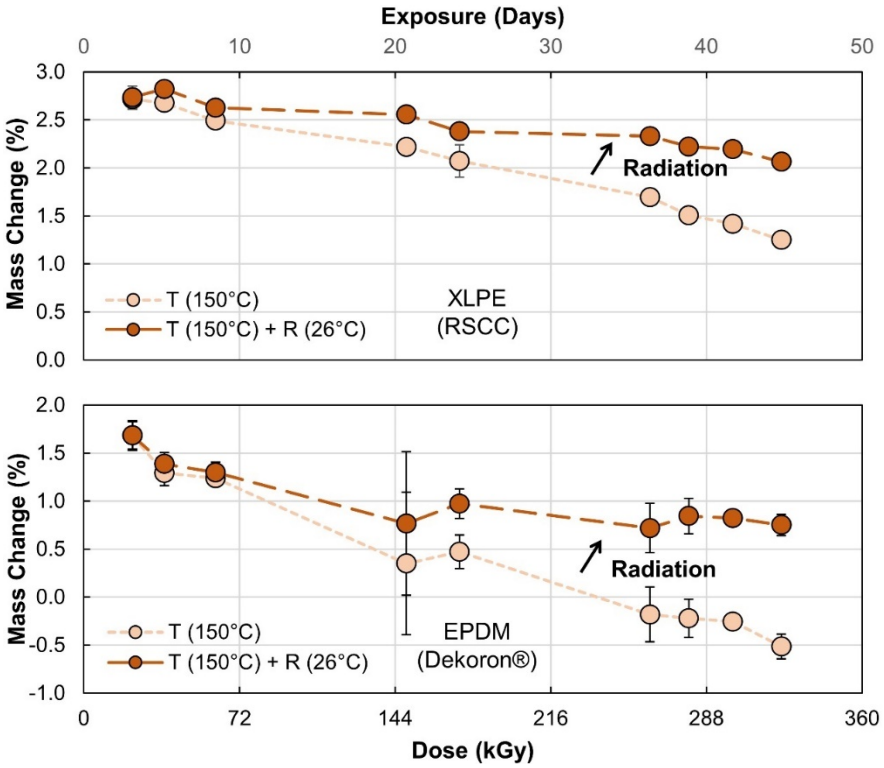

Figure 14. The average change in mass due to a radiation stressor (300 Gy/hr) after thermal aging (150°C) for (top) XLPE and (bottom) EPDM.

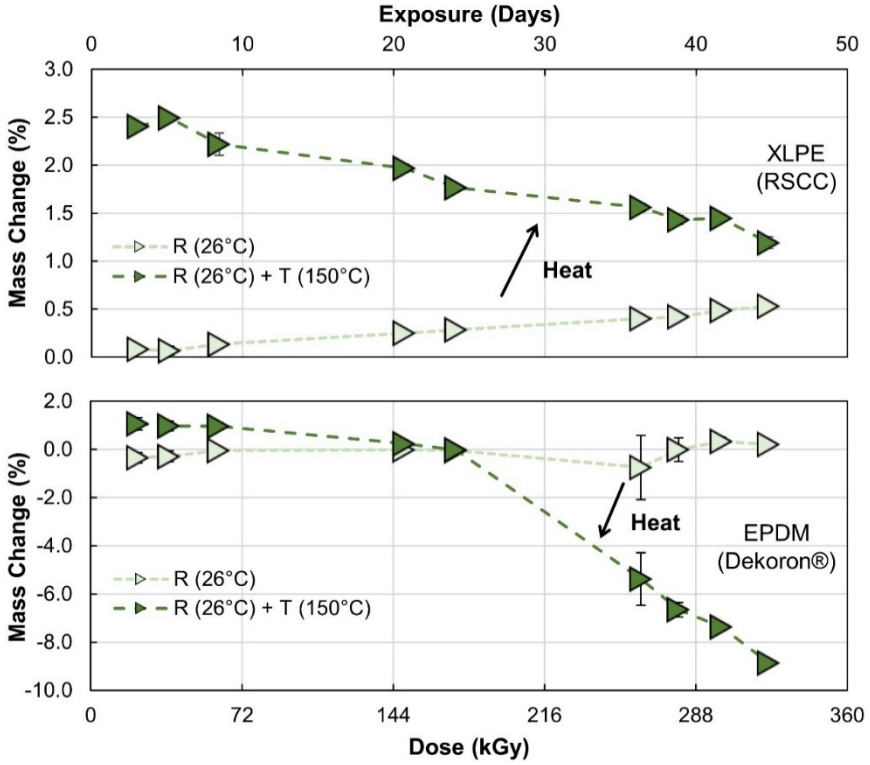

Figure 15. The average change in mass due to a thermal stressor (150°C) after irradiation (300 Gy/hr) for (top) XLPE and (bottom) EPDM.

6.2 Elongation at Break

The measured average EAB of the aged insulation specimens using video extensometry is shown in Figure 16. Parameters curve fit to Equation (9) are shown in Table 6. A sigmoidal, or S-shaped, curve [49] was observed for both material types and all three aging scenarios. The unaged XLPE specimens were likely not fully cured prior to aging because these specimens produced a reduced EAB (approximately 225%) when compared to the specimens at low exposure (3 days, 20 kGy, approximately 260% EAB). In this report, specimen end-of-life, or when the specimens were considered operationally degraded, was defined conservatively as 50% of the unaged EAB and to occur at the critical time, t_c [2]. Here, it was observed that the critical time depended both upon the aging scenario and material type. A critical time of 35 days (254 kGy) for the *T/R* aging scenario, 25 days (181 kGy) for the *T+R* aging scenario, and 41 days (300 kGy) for the *R+T* aging scenario was estimated for XLPE. Thus, for XLPE, the critical time of the *T+R* sequential aging scenario was estimated to be approximately 70% of the *T/R* simultaneous aging scenario. Because the simultaneous aging scenario may be more likely to occur in service, this result may indicate that laboratory sequential aging (thermal aging and then gamma irradiation [2]) may be conservative for XLPE in the prediction of cable lifetime. Also, the critical time of the *R+T* aging scenario was measured to be approximately 117% of that for the simultaneous aging scenario, possibly indicating that this aging sequence is less conservative for XLPE than what may occur under actual service conditions. In contrast, an opposite trend was measured for EPDM. Measured critical times of 27 days (196 kGy) for the *T/R* aging scenario, 30 days (218 kGy) for the *T+R* aging scenario, and 18 days (130 kGy) for the *R+T* aging scenario were estimated for EPDM. With EPDM, the lowest critical time was measured for the *R+T* aging scenario and was approximately 67% of that measured for the *T/R* simultaneous aging scenario. The laboratory aging scenario, *T+R*, produced an estimated critical time that was slightly greater than the *T/R* aging scenario (111%). The measured rate constants varied based upon material type and aging scenario. The measured rate constants for coupled temperature and radiation degradation have been estimated in the past as the superposition of the first-order, and non-interacting, rate constants for temperature and radiation, and an interacting rate constant [12]. Thus, comparison of the rate constants to literature is difficult.

Table 6. Evaluated EAB constants using Equation (9). Fitting was conducted using OriginPro® software to minimize the Chi-squared value.

Type	Aging Scenario	$e_{EAB,0}$ (%)	k (day^{-1})	t_c (day)
XLPE (RSCC)	*T/R*	266	-0.144	35.4
	T+R	252	-0.291	25.4
	R+T	263	-0.121	41.3
EPDM (Dekoron®)	*T/R*	391	-0.363	27.3
	T+R	431	-0.098	29.7
	R+T	408	-0.207	17.7

EPDM = ethylene-propylene-diene elastomer; XLPE = cross-linked polyethylene.

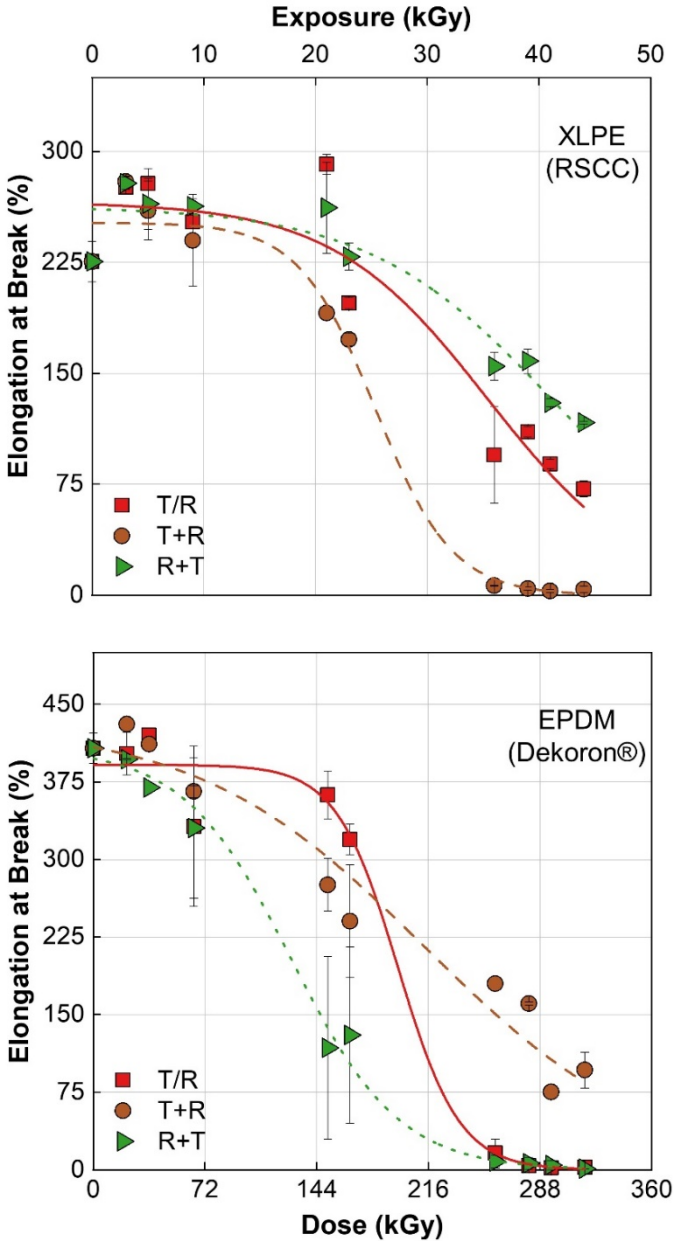

Figure 16. The average elongation at break analyzed using video extensometry for the aged (top) XLPE and (bottom) EPDM insulation specimens. A best fit of the data points using Equation (9) is shown.

6.3 Carbonyl Index

The measured FTIR ATR spectra for samples at selected absorbed doses are shown in Figures 17 and 18 for XLPE and EPDM, respectively. For increasing exposure (absorbed dose), stronger carbonyl absorption peaks (C=O, 1715 cm^{-1}) were measured for both material types and all aging scenarios, with the largest absorption occurring at the highest exposure (44 days, 320 kGy). Conversely, a decrease in the methylene absorption peak (C-H, 2848 cm^{-1}) was found for increasing exposure, with the smallest absorption occurring at the highest exposure. The relative change in the peak absorption for these functional groups was previously defined as the carbonyl index (vide supra) and is shown in Figure 19. The carbonyl index (CI) is a convenient metric for oxidation because the carbonyl groups are common oxidation byproducts and methylene groups form a common backbone for both XLPE and EPDM. Curve fitting parameters of the CI to the power law relationship of Equation (10) are shown in Table 7. For both material types and all aging scenarios, the CI increased with increasing exposure. A power law exponential (*b*) less than 1 was estimated for the XLPE specimens, possibly indicating that oxidation is limited with this material type, suggesting that the CI will plateau at higher exposures. A surprising result was observed for the XLPE specimens undergoing the *T*+*R* aging scenario. For XLPE and at the highest exposure of 44 days (320 kGy), the largest CI was measured for the *T/R* aging scenario (0.45), while the lowest CI was measured for the *T*+*R* aging scenario (0.23). However, for XLPE at this exposure, the specimens undergoing the *T*+*R* aging scenario appeared to be much more degraded (i.e., brittle) than the specimens undergoing the *T/R* aging scenario (4% EAB for the *T*+*R* specimens vs. 72% EAB for the *T/R* specimens); therefore, for the exposure conditions and dose rate explored here, this result may indicate that oxidation is not the primary degradation mechanism for XLPE. Conversely, the power law exponent was estimated to be greater than 1 for the EPDM specimens, similar to that observed in previous work [42]. Measurements of the CI for EPDM at 44 days of exposure were in line with expectations because the specimen with the highest CI (*R*+*T*, 2.5 at 320 kGy) correspondingly had the lowest EAB (1% EAB at 320 kGy), while the specimen with the lowest CI (*T*+*R*, 0.6 at 320 kGy) had the highest EAB (96% EAB at 320 kGy). Lastly, the constant *a* for EPDM and the *T*+*R* aging scenario was measured to be many orders of magnitude less than that for the other aging scenarios (10^{-14} for *T*+*R* vs. 10^{-5} for *T/R* and *R*+*T*). Because this constant is related to the concentration of hydrocarbons and the probability of oxidative reactions, and because the concentration of hydrocarbons is assumed to be constant between aging scenarios, it may be that the likelihood of degradation through oxidative pathways is greatly reduced for EPDM under the *T*+*R* aging scenario.

Table 7. Evaluated carbonyl index constants using Equation (10). Fitting was conducted using OriginPro® software to minimize the Chi-squared value.

Type	Aging Scenario	*a* (day^{-1})	*b* (a.u.)
XLPE (RSCC)	*T/R*	2.98×10^{-2}	0.736
	T+*R*	4.50×10^{-2}	0.443
	R+*T*	3.33×10^{-2}	0.553
EPDM (Dekoron®)	*T/R*	1.66×10^{-5}	3.09
	T+*R*	1.71×10^{-19}	11.3
	R+*T*	1.98×10^{-5}	3.19

a.u. = arbitrary units; EPDM = ethylene-propylene-diene elastomer; XLPE = cross-linked polyethylene.

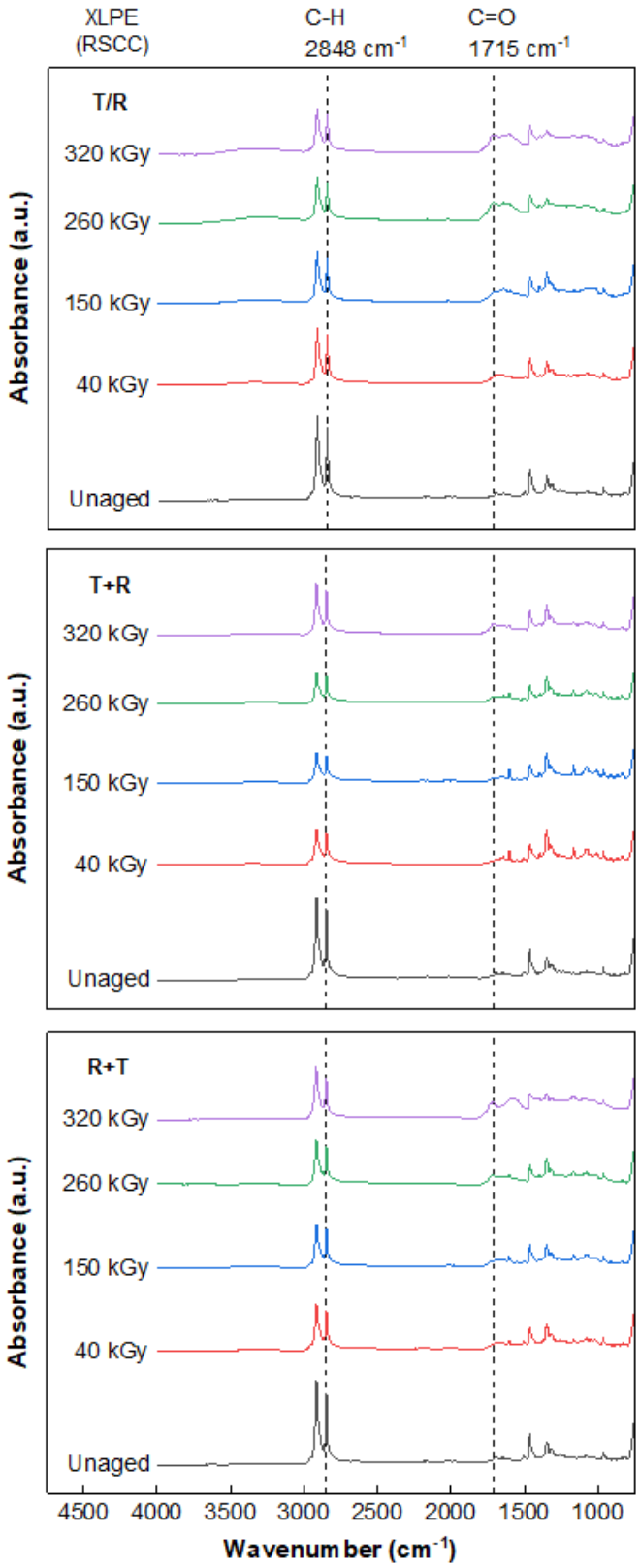

Figure 17. FTIR absorbance spectra for the XLPE insulation specimens. The carbonyl (1715 cm^{-1}) and methylene (2848 cm^{-1}) peaks are indicated.

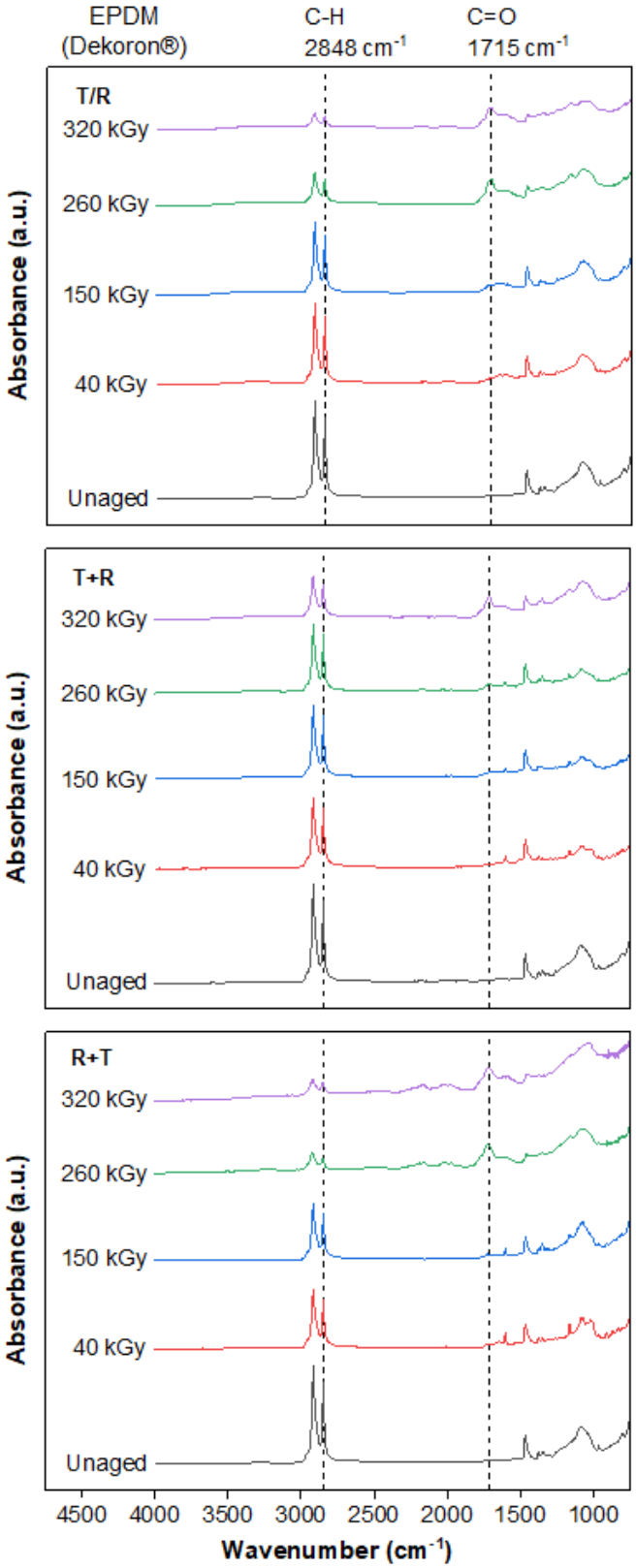

Figure 18. FTIR absorbance spectra for the EPDM insulation specimens. The carbonyl (1715 cm^{-1}) and methylene (2848 cm^{-1}) peaks are indicated.

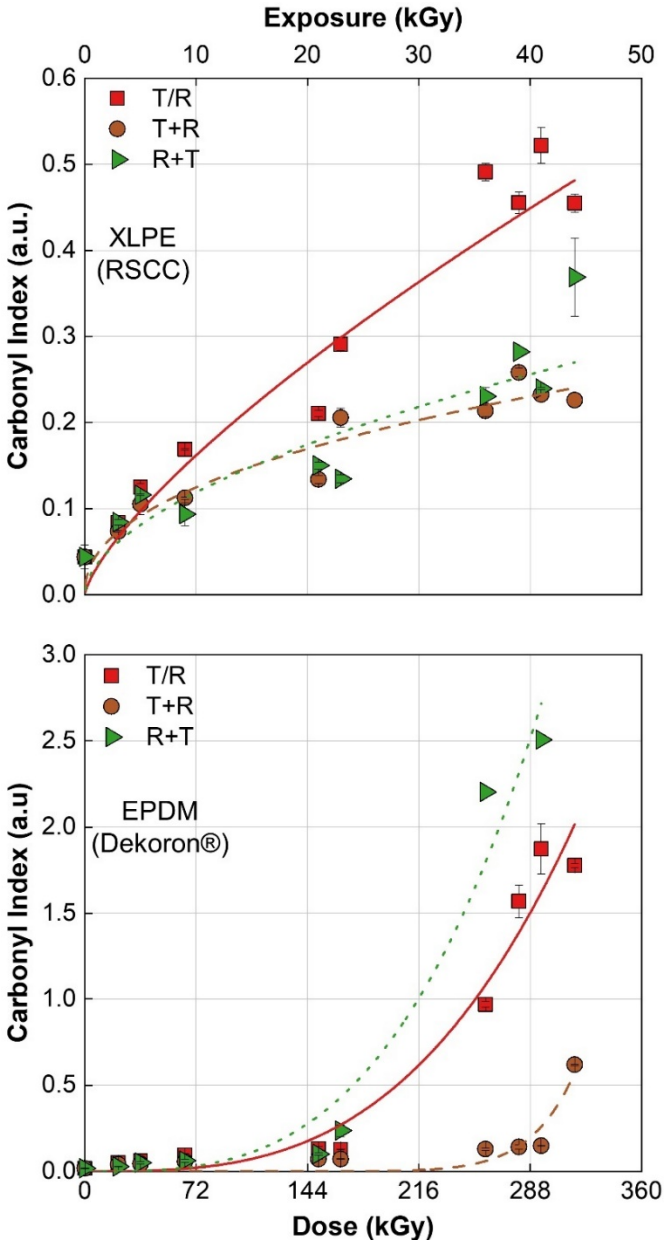

Figure 19. The average carbonyl index of the (top) XLPE and (bottom) EPDM insulation specimens after aging. A best fit of the data points using Equation (10) is shown.

6.4 Total Color Difference

Digital images of the aged insulation specimens at select exposures are shown in Figure 20. For both material types, increasing coloration of the insulation specimens was observed with increasing exposure; the XLPE specimens tended toward yellow and the EPDM specimens become darker (reddish). Therefore, it is likely that quantifying color change would have been more difficult using the yellowness index for the EPDM specimens. The total color difference approach incorporated here accounts for variations in specimen darkness, making this approach applicable for the current material types. The average total color difference for the insulation specimens is shown in Figure 21 for both material types and the evaluated parameters based upon Equation (11) are shown in Table 8. It should be noted that, due to the specimens being tubular in shape, reflection and shadowing on specimen surfaces produced scattering of the measured color data. Similar to that qualitatively apparent to the observer, the total color difference increased with increasing exposure, similar to that observed in previous work [50]. For XLPE, all aging scenarios appeared to converge, or plateau, at the equilibrium color difference ($\Delta E^*_{ab,\infty}$) at high exposures; for example, after 23 days of exposure (170 kGy) only small variations were measured in the total color difference for XLPE. However, differences were observed in the magnitude of the equilibrium color difference; the largest equilibrium color difference (23.2 for the *T+R* aging scenario) corresponded to the aging scenario that had the lowest EAB (4% EAB for the *T+R* aging scenario at 44 days exposure). Interestingly, the total color difference increased rapidly for the *R+T* aging scenario (XLPE), compared to the *T/R* or *T+R* aging scenarios, at low exposure; for example, at 3 days of exposure and 20 kGy dose, a ΔE^*_{ab} of 8.73, 9.45, and 15.4 was measured for the *T/R*, *T+R*, and *R+T* aging scenarios, respectively. Conversely, for EPDM, while the *T+R* aging scenario plateaued at approximately 23 days of exposure, both the *T/R* and *R+T* aging scenarios had yet to plateau for the exposures investigated. Even so, an equilibrium color difference was estimated based upon the fit curve: 37.6 for the *R+T* aging scenario and 33.0 for the *T/R* aging scenario, again in-line with expectations from EAB measurements. Similar to those observed for XLPE, the EPDM specimens demonstrated large color variations at low exposure for the *R+T* aging scenario: 12.8, 13.0, and 19.4 for the *T/R*, *T+R*, and *R+T* aging scenarios, respectively.

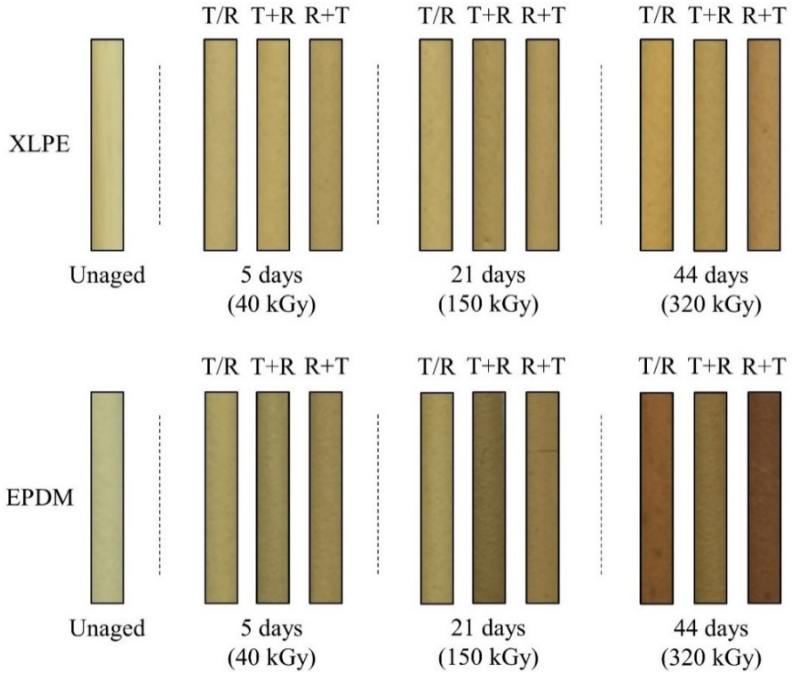

Figure 20. Original color digital images of the (top) XLPE and (bottom) EPDM specimens for select exposures.

Table 8. Evaluated total color difference constants using Equation (11). Fitting was conducted using OriginPro® software to minimize the Chi-squared value.

Type	Aging Scenario	$\Delta E^*_{ab,\infty}$ (a.u.)	c (a.u.)	τ (day^{-1})
XLPE (RSCC)	*T/R*	19.4	-13.2	7.04×10^{-2}
	T+R	23.2	-18.1	1.23×10^{-1}
	R+T	20.5	-14.9	3.60×10^{-1}
EPDM (Dekoron®)	*T/R*	33.0	-24.8	6.06×10^{-2}
	T+R	31.3	-27.1	1.88×10^{-1}
	R+T	37.6	-27.6	6.90×10^{-2}

a.u. = arbitrary units; EPDM = ethylene-propylene-diene elastomer; XLPE = cross-linked polyethylene.

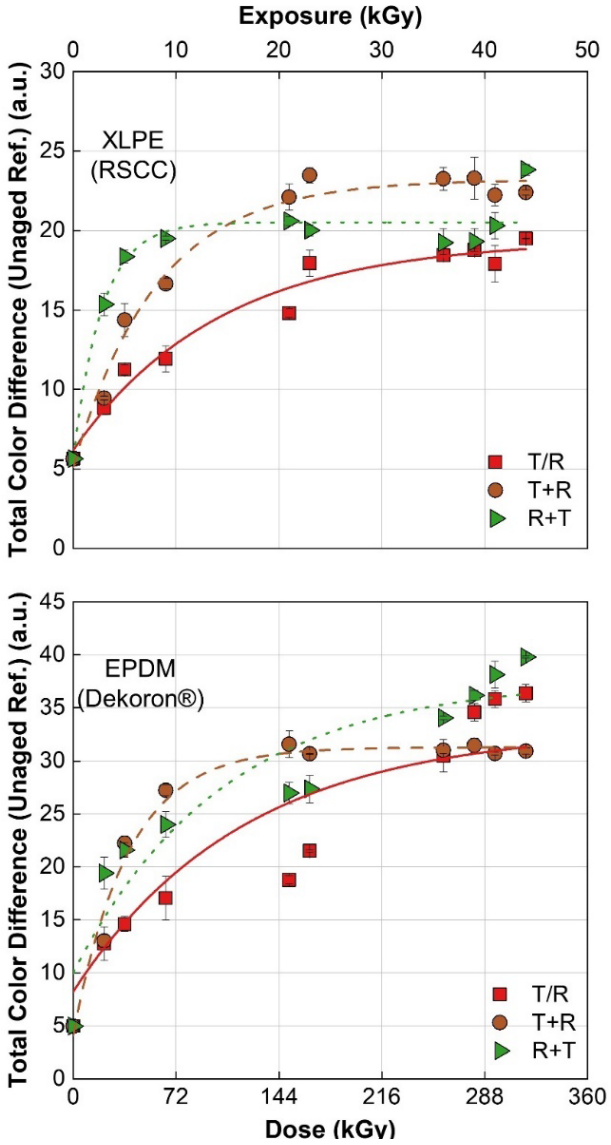

Figure 21. The average total color difference of the (top) XLPE and (bottom) EPDM insulation specimens after aging. A best fit of the data points using Equation (11) is shown.

7. DISCUSSION OF CHARACTERIZATION RESULTS

The generation of free radicals through thermal loads, radiation, mechanical forces, and/or catalysis [51] is a primary pathway for the degradation of polyolefin polymers by means of oxidative reactions. The process of free radical generation is partially self-sustaining in the presence of oxygen as additional free radicals are formed, some unstable [52] and others stable forming ketones (e.g. carbonyl groups). The reaction rate will increase with higher temperature and additional free radicals will be generated with increased irradiation due to an enhanced probability of chain scission. The propagation of this degradation process is much faster than the initiation [51], and this is especially true in the presence of antioxidants. For this reason, an induction time is commonly observed similar to that shown previously for EAB. In addition, the degradation rate of polymers at higher temperatures, or their thermal stability, also plays an important role [53] because the loss of mass can lead to early failure. In this report, a larger mass loss slope was measured for EPDM than for XLPE for the *T*+*R*, *R*+*T* and *T* aging scenarios. Similar to the loss observed in thermogravimetric analysis, the loss of mass is associated with the breakdown of the polymeric chains and the release of byproducts, whereas the initial increase of mass for the *T*+*R*, *R*+*T*, and *T* aging scenarios is hypothesized to be primarily due to thermo-oxidative reactions [54]. In terms of mass loss, the large decrease in measured mass for the EPDM *T/R* and *R*+*T* aging scenarios is of interest. As shown in Figure 22, the sharp decrease in mass is correlated with an EAB near 0% and indicates rapid degradation of the polymeric chains, with further degradation occurring as the mass continues to decrease. In contrast, all aging scenarios for XLPE and the *T*+*R* aging scenario for EPDM did not demonstrate a sharp decrease in mass even when the measured EAB was near 0% (e.g., at an exposure of 260 kGy or higher for the XLPE *T*+*R* aging scenario). As observed in previous work [55], this result may indicate that chain scission is the dominant mechanism for degradation of EPDM undergoing the *T/R* and *R*+*T* aging scenarios at high exposures. On the other hand, while the measured density variations (see Figure 23) for XLPE are hypothesized to be primarily due to oxidative reactions [2], the uncertainty regarding the CI results discussed in Section 6.3 make correlation of degradation for XLPE to a specific mechanism difficult.

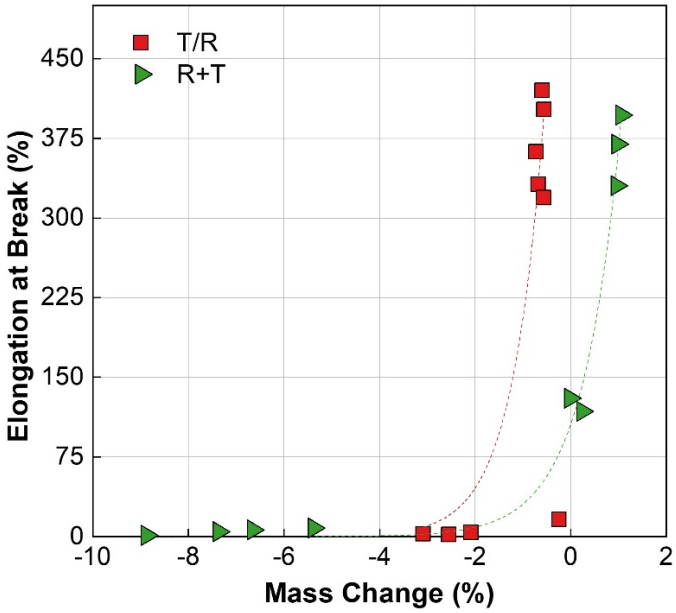

Figure 22. The elongation at break of the EPDM specimens vs. mass change; the dashed lines (---) are visual aids only

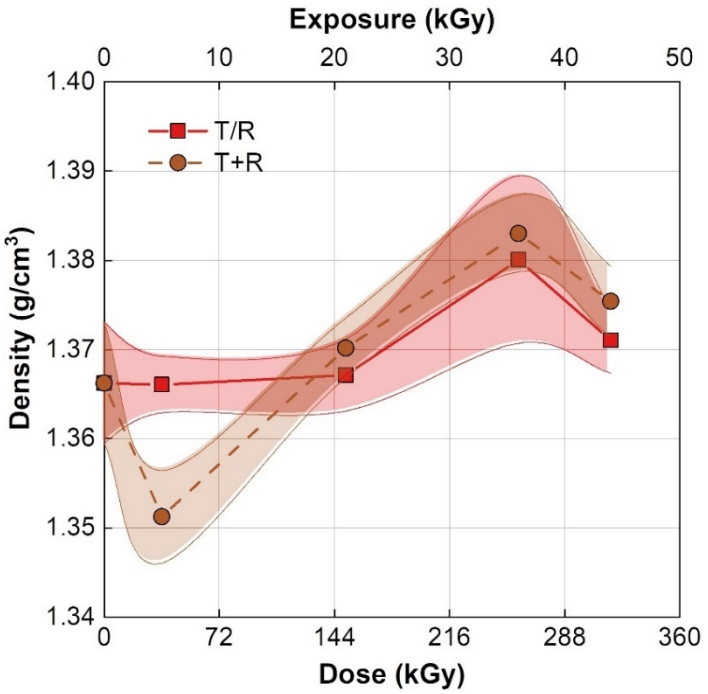

Figure 23. The average density of the XLPE insulation specimens after aging; the shaded regions represent the error bands.

Because EAB is a destructive measurement technique, previous work has looked into correlating EAB, a useful test metric to estimate the end of operational life (t_c) of polymeric specimens, with non-destructive measurement techniques. For example, it was previously observed that EAB correlated well with density measurements for some material types [56]; however, for XLPE and the *T/R* and *T+R* aging scenarios, no correlation was found between EAB and density. On the other hand, depending on the material type, correlation was observed between EAB and the CI or total color difference, both of which are non-destructive measurement techniques. The variation of EAB with respect to CI is shown in Figure 24 and with respect to total color difference in Figure 25. First, in regard to the CI and for XLPE, a linear trend was observed ($r^2 > 0.85$) for all aging scenarios and a lower EAB was correlated with a higher CI. However, no correlation was observed between the aging scenarios and the critical time based upon the slope of the linear line; that is, a shallower slope, or higher CI at increased exposures, did not indicate that the critical time was reduced (as previously discussed in Section 6.3). Second, both the CI for EPDM (see Figure 24) and the total color difference for XLPE (see Figure 25) demonstrate exponential variations with EAB for all aging scenarios. However, these test metrics are a poor choice for the specified materials because they have a weak correlation to EAB and relatively insensitive variations for a large range of test measurements. Third, the total color difference for EPDM exhibited a sigmoidal trend ($r^2 > 0.90$ for *T/R* and *R+T*, and $r^2 > 0.72$ for *T+R*) for all aging scenarios. Interestingly, the exposure corresponding to the critical total color difference (the total color difference where EAB was half its initial value in Figure 25) was approximately 65% (± 4.6%) of the critical time measured for EAB in Table 6. Therefore, based upon the above discussion, the CI for XLPE and the total color difference for EPDM may be useful non-destructive techniques to evaluate the critical time of cable insulation in the field. Furthermore, measurement of the total color difference is a particularly advantageous technique because a trained individual can distinguish variations in total color difference in the range of 0.1 to 0.2 [57]; however, the prevalence of darker color cable insulation limits the applicability of this technique.

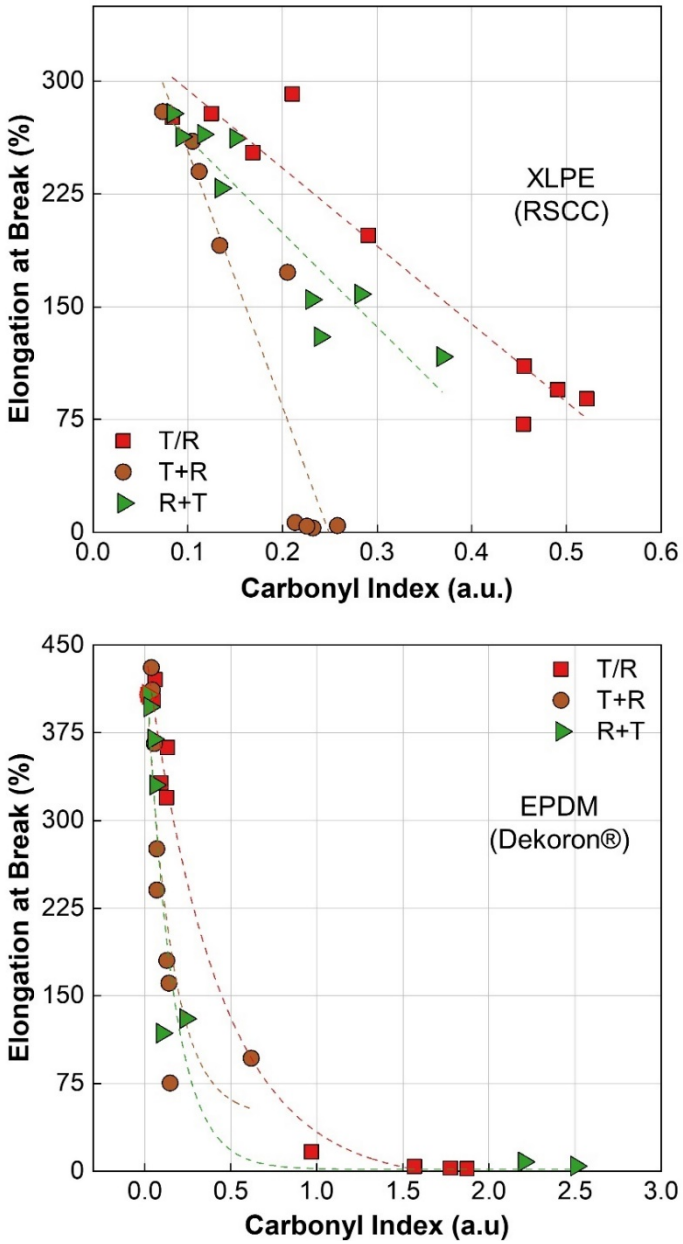

Figure 24. Variations in the elongation at break with respect to the carbonyl index for (top) XLPE and (bottom) EPDM; the dashed lines (---) are visual aids only.

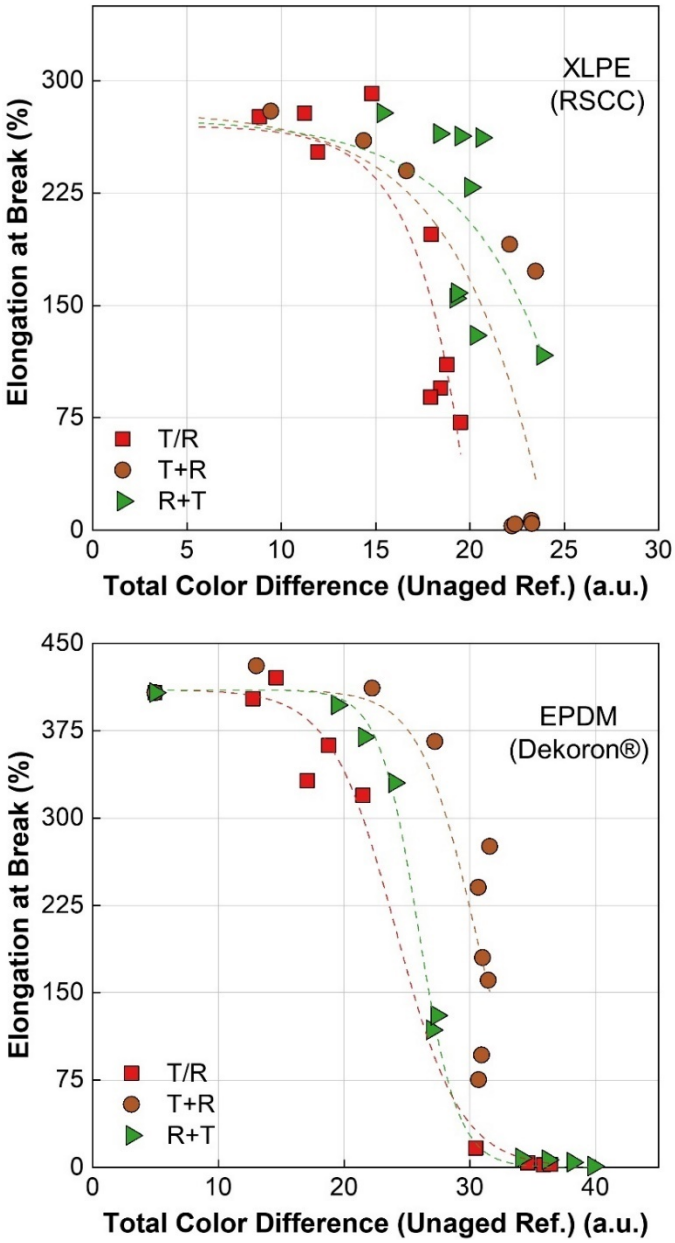

Figure 25. Variations in the elongation at break with respect to total color difference for (top) XLPE and (bottom) EPDM; the dashed lines (---) are visual aids only.

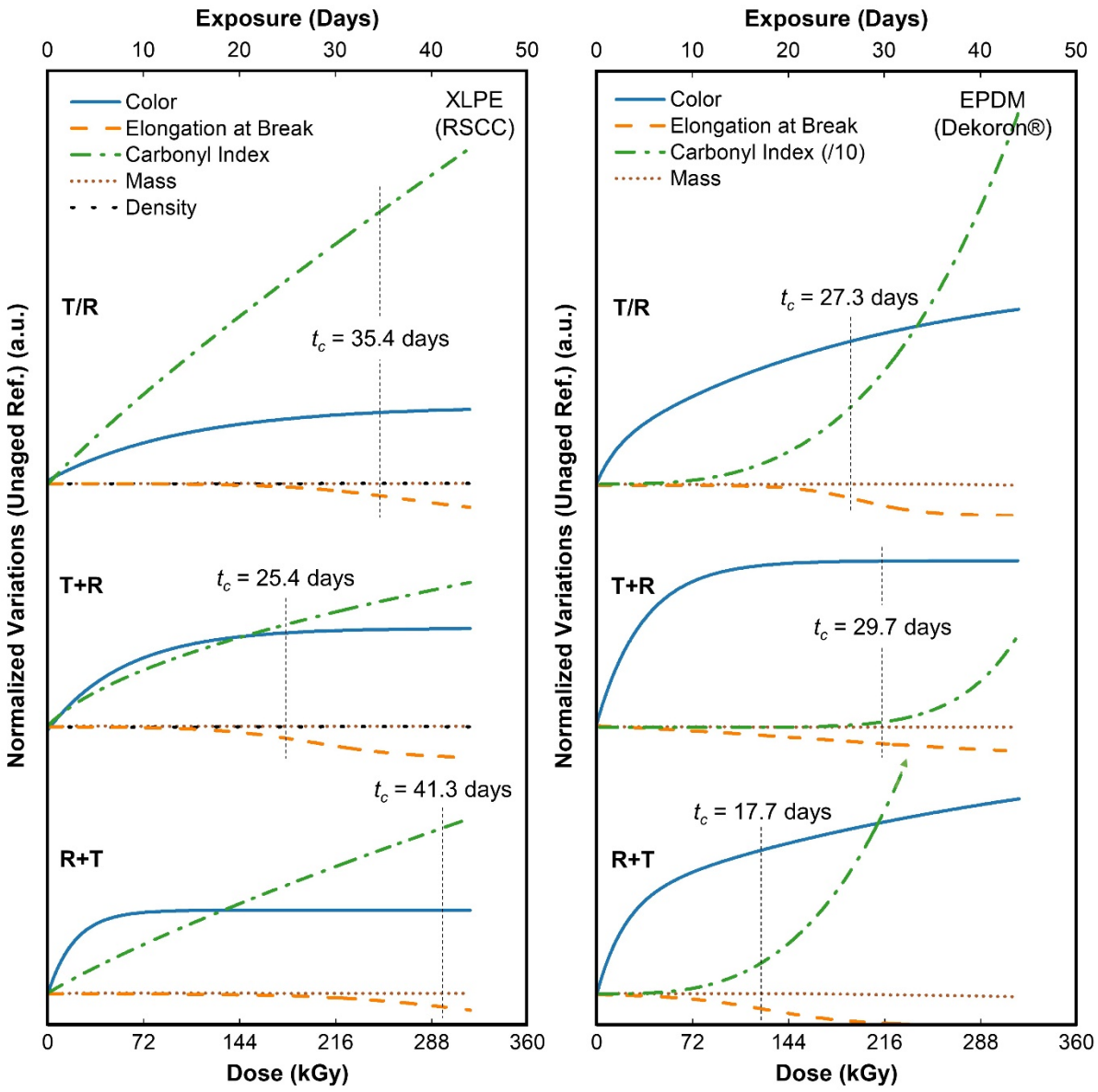

Figure 26. Normalized variations in the measured properties for aged insulation specimens: (left) XLPE and (right) EPDM. The critical time (t_c), representing 50% of initial EAB, is indicated on the figures.

In addition to metrics that correlate well to existing standards for cable degradation, such as EAB, preferred characterization techniques are sensitive to cable degradation [58]. In this report, the sensitivity of the characterization technique is defined as the ratio of the aged specimen property to the unaged specimen property; thus, as cable specimens age, sensitive characterization techniques produce larger normalized variations in measured properties. The normalized, curve fit, variations of the test metrics employed in this report are shown Figure 26. Here, as opposed to EAB, it was observed that the CI was the most sensitive test metric, followed by the total color difference. However, plateauing of the total color difference for XLPE and the exponential trend of CI for EPDM make correlation to degradation difficult. In all aging scenarios and for both material types, mass change and density were the least sensitive characterization techniques. Therefore, the most sensitive and possibly most appropriate characterization techniques are the CI for XLPE and total color difference for EPDM, similar to that found for correlation to EAB above.

8. CONCLUSIONS

The objective of this report was to address one of the four cable aging knowledge gaps, synergistic effects, emphasized by Fifield et al. [7]. Synergistic effects were defined as polymer aging mechanisms due to simultaneous or concurrent application of thermal and gamma radiation stressors, which may differ from sequentially applied thermal and gamma radiation stressors. Previously, it was suggested that cable degradation was more severe with simultaneous aging than with sequential aging [4]. Therefore, there has been concern that the historical practice of applying sequential aging (thermal followed by irradiation) [2] to estimate cable lifetimes may not accurately reflect in-service conditions where cables may experience both high temperatures and radiation exposure simultaneously.

In this report, two of the most common cable insulation materials in nuclear containment (XLPE and EPDM) low-voltage cables were selected to assess the accuracy of the findings. Accelerated aging experiments were conducted while holding the dose rate and temperature constant to better understand cable degradation based upon the order of the sequence of the stressor. Furthermore, the dose rate, total dose, and temperature were selected based upon input from multiple expert stakeholders and experimental constraints. Characterization methods that included mass change, elongation at break, carbonyl index, total color difference and density were selected to quantify the severity of the selected aging scenarios: (1) simultaneous [*T/R*, thermal and irradiation], (2) sequential [*T*+*R*, thermal followed by irradiation], and (3) sequential [*R*+*T*, irradiation followed by thermal].

The characterization results have yielded insights into lifetime predictions of low-voltage nuclear instrumentation cables. Most significantly, sequential aging was found to produce a significantly different operational lifetime (defined as time to 50% of the unaged specimen EAB) when compared to simultaneous aging dependent upon the material type and aging scenario as shown below in Table 9. For XLPE, lifetimes were found to be less than the simultaneous aging scenario for the sequential thermal followed by irradiation aging, but greater for the sequential irradiation followed by thermal aging. Conversely, for EPDM, lifetimes were found to be less than the simultaneous aging scenario for sequential irradiation followed by thermal aging, but greater for sequential thermal followed by irradiation aging. This report has also demonstrates that mass change may be a useful technique for estimating the degradation of cables insulated with EPDM, particularly with the simultaneous (*T/R*) and sequential irradiation followed by thermal (*R*+*T*) aging scenarios, because a sharp decrease in mass was observed to correlate to a reduction in EAB. In addition, the CI for XLPE and the total color difference for EPDM were observed to be possibly advantageous non-destructive characterization methods for estimating cable insulation lifetimes.

Table 9. Lifetime prediction of sequential aging scenarios normalized to the simultaneous aging scenario.

Type	Aging Scenario	Lifetime with respect to Simultaneous (*T/R*) (%)
XLPE (RSCC)	*T*+*R*	72
	R+*T*	117
EPDM (Dekoron®)	*T*+*R*	109
	R+*T*	65

EPDM = ethylene-propylene-diene elastomer; XLPE = cross-linked polyethylene.

Future work will consider additional measures of the aging of XLPE and EPDM cable materials, including indenter modulus and oxidation induction time. Similar analysis of additional low-voltage cable insulation materials aged under the same conditions described here will be performed to determine material-specific trends in aging sequence dependence.

9. REFERENCES

[1] P.L. Joskow, The Future of nuclear power in the United States: Economic and regulatory challenges, (2006).

[2] M. Subudhi, Literature Review of Environmental Qualification of Safety-Related Electric Cable, 1 (1996) 1–306. http://www.iaea.org/inis/collection/NCLCollectionStore/_Public/27/059/27059900.pdf.

[3] R.F. Gazdzinski, W.M. Denny, G.J. Toman, R.T. Butwin, SAND96-0344: Aging Managment Guideline for Commercial Nuclear Power Plants - Electrical Cble and Terminations, 2000.

[4] NRC, Expanded Materials Degradation Assessment (EMDA), Volume 5: Aging of Cables and Cable Systems, NUREG/CR-7153, 2014.

[5] Nuclear Energy Agency - Committee on the Safety of Nuclear Installations, NEA/CSNI/R(2018)8 Cable Ageing in Nuclear Power Plants, 2018.

[6] PNNL, Light Water Reactor Sustainability (LWRS) Program–Non-Destructive Evaluation (NDE) R&D Roadmap for Determining Remaining Useful Life of Aging Cables in Nuclear Power Plants, PNNL-21731. (2012).

[7] L.S. Fifield, A. Zwoster, M. Murphy, PNNL-27987: Initiation of Experimental Campaign to Address Knowledge Gaps Related to Simultaneous Thermal and Gamma Radiation Aging of Crosslinked Polyethylene and Ethylene-Propylene Rubber Cable Insulation, Richland, WA, 2018.

[8] K.T. Gillen, R.L. Clough, Rigorous experimental confirmation of a theoretical model for diffusion-limited oxidation, Polymer (Guildf). 33 (1992) 4358–4365. https://doi.org/10.1016/0032-3861(92)90280-A.

[9] L. Verardi, D. Fabiani, G.C. Montanari, Correlation of electrical and mechanical properties in accelerated aging of LV nuclear power plant cables, ICHVE 2014 - 2014 Int. Conf. High Volt. Eng. Appl. (2014) 1–4. https://doi.org/10.1109/ICHVE.2014.7035376.

[10] K.T. Gillen, R.L. Clough, Time-temperature-dose rate superposition: A methodology for extrapolating accelerated radiation aging data to low dose rate conditions, Polym. Degrad. Stab. 24 (1989) 137–168. https://doi.org/10.1016/0141-3910(89)90108-0.

[11] G. Przybytniak, J. Boguski, V. Placek, L. Verardi, D. Fabiani, E. Linde, U.W. Gedde, Inverse effect in simultaneous thermal and radiation aging of EVA insulation, Express Polym. Lett. 9 (2015) 384–393. https://doi.org/10.3144/expresspolymlett.2015.36.

[12] K.T. Gillen, Importance of Synergism for Degradation of Elastomers in Combined Radiation Plus Temperature Environments, Rubber Chem. Technol. 93 (2019) 121–141. https://doi.org/10.5254/rct.19.80457.

[13] T. Seguchi, K. Tamura, T. Ohshima, A. Shimada, H. Kudoh, Degradation mechanisms of cable insulation materials during radiation-thermal ageing in radiation environment, Radiat. Phys. Chem. 80 (2011) 268–273. https://doi.org/10.1016/j.radphyschem.2010.07.045.

[14] T. Seguchi, K. Tamura, H. Kudoh, A. Shimada, M. Sugimoto, Degradation of cable insulation material by accelerated thermal radiation combined ageing, IEEE Trans. Dielectr. Electr. Insul. 22 (2015) 3197–3206. https://doi.org/10.1109/TDEI.2015.004880.

[15] M. Ito, Service Life Prediction of Polymeric Materials, Springer US, Boston, MA, 2009. https://doi.org/10.1007/978-0-387-84876-1.

[16] M.T. Shaw, Y.M. Liu, Modeling of thermal and radiative aging of polymeric cable materials, Conf. Rec. IEEE Int. Symp. Electr. Insul. 2 (1996) 638–641. https://doi.org/10.1109/elinsl.1996.549426.

[17] DOE, Aging management guideline for commercial nuclear power plants - electrical cable and terminations, SAND96-0344. (1996). http://www.osti.gov/energycitations/product.biblio.jsp?osti_id=204243.

[18] ASTM, D1418 Standard Practice for Rubber and Rubber Latices - Nomenclature, West Conshohocken, PA, 2017. https://doi.org/10.1520/D1418-17.

[19] M.F. Sheridan, ed., The Vanderbilt Rubber Handbook, 14th Edition, R. T. Vanderbilt, Norwalk,

CT, 2010.
[20] P. Hu, P.P. Zhao, G.W. Zhang, X.H. Wang, Thermal properties of 60Co irradiated crosslinked high density polyethylene, Sol. Energy Mater. Sol. Cells. 149 (2016) 55–59. https://doi.org/10.1016/j.solmat.2015.12.042.
[21] A.R. Amin, Synergistic effect of TNPP and carbon black in weathered XLPE materials, J. Polym. Environ. 17 (2009) 267–272. https://doi.org/10.1007/s10924-009-0148-5.
[22] R. Kochetov, T. Christen, F. Gullo, FTIR analysis of LDPE and XLPE thin samples pressed between different protective anti-Adhesive films, ICEMPE 2017 - 1st Int. Conf. Electr. Mater. Power Equip. (2017) 49–52. https://doi.org/10.1109/ICEMPE.2017.7982097.
[23] Q. Zhao, X. Li, J. Gao, Aging of ethylene-propylene-diene monomer (EPDM) in artificial weathering environment, Polym. Degrad. Stab. 92 (2007) 1841–1846. https://doi.org/10.1016/j.polymdegradstab.2007.07.001.
[24] M. Tefferi, Z. Li, Y. Cao, H. Uehara, Q. Chen, Novel EPR-insulated DC cables for future multi-terminal MVDC integration, IEEE Electr. Insul. Mag. 35 (2019) 20–27. https://doi.org/10.1109/MEI.2019.8804331.
[25] F.J. Linnig, J.E. Stewart, Infrared study of some structural changes in natural rubber during vulcanization, J. Res. Natl. Bur. Stand. (1934). 60 (1958) 9. https://doi.org/10.6028/jres.060.002.
[26] L. Guadagno, P. Longo, M. Raimondo, C. Naddeo, A. Mariconda, V. Vittoria, G. Iannuzzo, S. Russo, Use of Hoveyda-Grubbs' second generation catalyst in self-healing epoxy mixtures, Compos. Part B Eng. 42 (2011) 296–301. https://doi.org/10.1016/j.compositesb.2010.10.011.
[27] S. Mitra, A. Ghanbari-Siahkali, P. Kingshott, S. Hvilsted, K. Almdal, An investigation on changes in chemical properties of pure ethylene-propylene-diene rubber in aqueous acidic environments, Mater. Chem. Phys. 98 (2006) 248–255. https://doi.org/10.1016/j.matchemphys.2005.09.028.
[28] L. Greenspan, Humidity fixed points of binary saturated aqueous solutions, J. Res. Natl. Bur. Stand. Sect. A Phys. Chem. 81A (1977) 89. https://doi.org/10.6028/jres.081A.011.
[29] IEC/IEEE 62582-3: 2012, Nuclear power plants - Instrumentation and control important to safety - Electrical equipment condition monitoring methods - Part 3: Elongation at break, International Electrotechnical Commission, Geneva, Switzerland, 2012. https://doi.org/10.3403/30189461.
[30] S.G. Kazarian, K.L.A. Chan, ATR-FTIR spectroscopic imaging: Recent advances and applications to biological systems, Analyst. 138 (2013) 1940–1951. https://doi.org/10.1039/c3an36865c.
[31] D. Fassini, A.R.C. Duarte, R.L. Reis, T.H. Silva, Bioinspiring chondrosia reniformis (Nardo, 1847) collagen-based hydrogel: A new extraction method to obtain a sticky and self-healing collagenous material, Mar. Drugs. 15 (2017). https://doi.org/10.3390/md15120380.
[32] P.S. Thomas, J.P. Guerbois, G.F. Russell, B.J. Briscoe, FTIR study of the thermal degradation of poly(vinyl alcohol), J. Therm. Anal. Calorim. 64 (2001) 501–508. https://doi.org/10.1023/A:1011578514047.
[33] J. Troscianko, Empirical Imaging, (2020). http://www.empiricalimaging.com/ (accessed January 23, 2020).
[34] J. Troscianko, M. Stevens, Image calibration and analysis toolbox - a free software suite for objectively measuring reflectance, colour and pattern, Methods Ecol. Evol. 6 (2015) 1320–1331. https://doi.org/10.1111/2041-210X.12439.
[35] S.A. Burns, Generating Reflectance Curves from sRGB Triplets, (2017) 1–39. http://scottburns.us/reflectance-curves-from-srgb/.
[36] ASTM D792-13, Standard Test Methods for Density and Specific Gravity (Relative Density) of Plastics by Displacement, West Conshohocken, PA, 2013. https://doi.org/10.1520/D0792-13.2.
[37] S. Liu, L.S. Fifield, N. Bowler, Aging mechanisms and nondestructive aging indicator of filled cross-linked polyethylene (XLPE) exposed to simultaneous thermal and gamma radiation, Miner. Met. Mater. Ser. (2019) 1281–1291. https://doi.org/10.1007/978-3-030-04639-2_82.
[38] B. Moon, N. Jun, S. Park, C.S. Seok, U.S. Hong, A study on the modified Arrhenius equation using the oxygen permeation block model of crosslink structure, Polymers (Basel). 11 (2019). https://doi.org/10.3390/polym11010136.

[39] L.A. Jirackova, J. Verdu, Chemiluminescence of hydrocarbon polymers, J. Polym. Sci. Part A Polym. Chem. 25 (1987) 1205–1217. https://doi.org/10.1002/pola.1987.080250502.
[40] M. Celina, G.A. George, Heterogeneous and homogeneous kinetic analyses of the thermal oxidation of polypropylene, Polym. Degrad. Stab. 50 (1995) 89–99. https://doi.org/10.1016/0141-3910(95)00136-A.
[41] K.T. Gillen, M. Celina, Predicting Polymer Degradation and Mechanical Property Changes for Combined Aging Environments, in: Fall 190th Tech. Meet. Rubber Div. ACS, Pittsburgh, PA, 2016.
[42] F. Gugumus, Thermooxidative degradation of polyolefins in the solid state: Part 1. Experimental kinetics of functional group formation, Polym. Degrad. Stab. 52 (1996) 131–144. https://doi.org/10.1016/0141-3910(95)00229-4.
[43] N.M. Emanuel, Thermo-oxidative ageing of polymers, Polym. Sci. U.S.S.R. 27 (1985) 1505–1525. https://doi.org/10.1016/0032-3950(85)90340-5.
[44] L. Audouin, V. Langlois, J. Verdu, J.C.M. de Bruijn, Role of oxygen diffusion in polymer ageing: kinetic and mechanical aspects, J. Mater. Sci. 29 (1994) 569–583. https://doi.org/10.1007/BF00445968.
[45] W. Schnabel, ed., Polymers and Electromagnetic Radiation, Wiley-VCH Verlag GmbH & Co. KGaA, Weinheim, Germany, 2014. https://doi.org/10.1002/9783527677719.
[46] S.A. Nouh, A. Mohamed, R.A. Bahareth, M.M. Abutalib, K. Benthami, Color changes in X-ray irradiated PM-355 and Makrofol DE 7-2 nuclear track detectors, Eur. Phys. J. Appl. Phys. 65 (2014) 30201. https://doi.org/10.1051/epjap/2014130422.
[47] L. Boukezzi, A. Boubakeur, Prediction of mechanical properties of XLPE cable insulation under thermal aging: Neural network approach, IEEE Trans. Dielectr. Electr. Insul. 20 (2013) 2125–2134. https://doi.org/10.1109/TDEI.2013.6678861.
[48] B.R. Crenshaw, M. Burnworth, D. Khariwala, A. Hiltner, P.T. Mather, R. Simha, C. Weder, Deformation-induced color changes in mechanochromic polyethylene blends, Macromolecules. 40 (2007) 2400–2408. https://doi.org/10.1021/ma062936j.
[49] M. Rahaman, A. Aldalbahi, P. Govindasami, N.P. Khanam, S. Bhandari, P. Feng, T. Altalhi, A new insight in determining the percolation threshold of electrical conductivity for extrinsically conducting polymer composites through different sigmoidal models, Polymers (Basel). 9 (2017) 1–17. https://doi.org/10.3390/polym9100527.
[50] R. Steffen, H. Setyamukti, G. Wallner, K. Geretschläger, B. Röder, Kinetics of degradation-induced polymer luminescence: Polyamide under dry heat exposure, Polym. Degrad. Stab. 140 (2017) 114–125. https://doi.org/10.1016/j.polymdegradstab.2017.04.010.
[51] S. Liu, S.W. Veysey, L.S. Fifield, N. Bowler, Quantitative analysis of changes in antioxidant in crosslinked polyethylene (XLPE) cable insulation material exposed to heat and gamma radiation, Polym. Degrad. Stab. 156 (2018) 252–258. https://doi.org/10.1016/j.polymdegradstab.2018.09.011.
[52] G. Teissedre, J.F. Pilichowski, S. Chmela, J. Lacoste, Ageing of EPDM - I: Photo and thermal stability of EPDM hydroperoxides, Polym. Degrad. Stab. 53 (1996) 207–215. https://doi.org/10.1016/0141-3910(96)00082-1.
[53] Y.S. Cho, M.J. Shim, S.W. Kim, Thermal degradation kinetics of PE by the Kissinger equation, Mater. Chem. Phys. 52 (1998) 94–97. https://doi.org/10.1016/S0254-0584(98)80013-8.
[54] B. Gewert, M.M. Plassmann, M. Macleod, Pathways for degradation of plastic polymers floating in the marine environment, Environ. Sci. Process. Impacts. 17 (2015) 1513–1521. https://doi.org/10.1039/c5em00207a.
[55] A. Kömmling, M. Jaunich, D. Wolff, Revealing effects of chain scission during ageing of EPDM rubber using relaxation and recovery experiment, Polym. Test. 56 (2016) 261–268. https://doi.org/10.1016/j.polymertesting.2016.10.026.
[56] J. V. Gasa, Z. Liu, M.T. Shaw, Relationship between density and elongation-at-break of naturally and artificially aged cable materials used in nuclear power plants, Polym. Degrad. Stab. 87 (2005)

77–85. https://doi.org/10.1016/j.polymdegradstab.2004.07.009.
[57] G. Iannuzzi, B. Mattsson, M. Rigdahl, Color changes due to thermal ageing and artificial weathering of pigmented and textured ABS, Polym. Eng. Sci. 53 (2013) 1687–1695. https://doi.org/10.1002/pen.23438.
[58] F.M. Guérout, R.G. Boor, Development of indentation techniques in support of cable condition monitoring programs, IEEE Trans. Dielectr. Electr. Insul. 22 (2015) 2818–2825. https://doi.org/10.1109/TDEI.2015.004612.